3 1176 00518 2283

NASA-CR-172,429

NASA Contractor Report 172429

NASA-CR-172429
19840025110

DEFINITION, ANALYSIS AND DEVELOPMENT OF AN OPTICAL DATA DISTRIBUTION NETWORK FOR INTEGRATED AVIONICS AND CONTROL SYSTEMS

PART II: COMPONENT DEVELOPMENT AND SYSTEM INTEGRATION

H.W. Yen and R.J. Morrison

Hughes Research Laboratories
3011 Malibu Canyon Road
Malibu, CA 90265

NAS1–15829
Final Report
1 May 1979 through 31 March 1984

June 1984

LIBRARY COPY

SEP 27 1984

LANGLEY RESEARCH CENTER
LIBRARY, NASA
HAMPTON, VIRGINIA

NASA
National Aeronautics and
Space Administration

Langley Research Center
Hampton, Virginia 23665

TABLE OF CONTENTS

SECTION		PAGE
1	INTRODUCTION AND SUMMARY	1-1
2	REVIEW OF WAVELENGTH DIVISION MULTIPLEXING ..	2-1
	A. Angular Dispersive Devices	2-2
	B. Interference Filters	2-6
3	PLANAR ROWLAND SPECTROMETER AS A DEMULTIPLEXER	3-1
	A. Principle of Operation	3-1
	B. First Generation Devices	3-4
4	IMPROVED DEMULTIPLEXER DESIGN	4-1
	A. Device Design	4-2
	B. Aberration of the Device	4-4
	C. Waveguide Dispersion	4-8
5	DEMULTIPLEXER FABRICATION AND TESTING	5-1
	A. Waveguide Fabrication and Characterization	5-1
	B. Grating Fabrication and Testing	5-7
	C. Demultiplexer Packaging and Characterization	5-14
6	FABRICATION OF 4 X 4 STAR COUPLERS	6-1
7	DISCUSSIONS AND CONCLUSIONS	7-1
8	REFERENCES	8-1

N84-33181#

LIST OF ILLUSTRATIONS

FIGURE		PAGE
1-1	Wavelength Multiplexing Data Bus	1-3
1-2	Schematic of a planar Roland spectrometer	1-4
1-3	The multiplexer and demultiplexers with fiber cable interconnections	1-5
2-1	Block diagram of a typical wavelength division multiplexing system. (a) Single-fiber one-directional transmission, (b) two-fiber bidirectional transmission, and (c) single-fiber bidirectional transmission	2-3
2-2	Examples of demultiplexers using diffraction gratings. (a) A bulk approach, and (b) a planar approach	2-5
2-3	Examples of demultiplexers using interference filters. (a) A simple two-channel demultiplexer. (b) A multi-channel multiplexer-demultiplexer	2-7
3-1	Illustration of the Rowland circle principle	3-2
3-2	Intensity profile at the output face with 55 μm core input fiber excitation; (a) using He-Ne laser, λ = 6328 Å; (b) using semi-conductor laser, λ = 8255 Å	3-6
3-3	Experimental arrangement for demultiplexer characterization	3-8
3-4(a)	Demultiplexer output as a function of output fiber position. The solid curves were taken with both lasers on simultaneously; the broken curves were taken with one laser on at a time. The two peaks correspond to λ = 8255 Å and λ = 8455 Å	3-9
3-4(b)	Demultiplexer output as a function of output fiber position. The solid curves were taken with both lasers on simultaneously, the broken curves were taken with one laser on at a time. (b) The two peaks correspond to λ = 8312 Å and λ = 8410 Å	3-10

LIST OF ILLUSTRATIONS (CONT)

FIGURE		PAGE
4-1	Planar Roland spectrometer with modified structure	4-1
4-2	Relations between the incident angle α and the diffracted angle β	4-3
4-3	Geometrical illustration of the inherent aberration associated with a Roland spectrometer	4-5
4-4	The condition for minimum aberration is that the grating period along the arc varies as $d = d_o/\cos\phi$	4-8
4-5	A vector diagram illustrating the diffraction of two waves with unequal wave vector	4-10
4-6	A waveguide structure in which the guiding layer thickness varies adiabatically from t_1 to t_2	4-12
4-7	The effective mode index of each guided TE mode varies when the waveguide thickness is under adiabatic transition in its thickness ..	4-13
4-8	The calculated output spot profile of a modified Rowland spectrometer when illuminated by a 55 μm source of uniform intensity and phase	4-15
5-1	The tapered waveguide used in the experiment. The numbers shown indicate the actual waveguide thickness	5-2
5-2	Experimental setup for observing the collimating effect of tapered waveguide	5-2
5-3	Demultiplexer waveguide geometry	5-6
5-4	Relations of α, β, and Θ	5-9
5-5	Dimensions of the concave grating	5-10

LIST OF ILLUSTRATIONS (CONCLUDED)

FIGURE		PAGE
5-6	Grating geometry and locations of various defects	5-10
5-7	Demultiplexer Housing	5-13
5-8	Optical power versus output fiber location trace for W - 5	5-15
5-9	Optical power versus output fiber location trace for W - 9	5-16
5-10	Optical power versus output fiber location trace for W - 3	5-17
5-11	Optical power versus output fiber location trace for W - 6	5-18
5-12	Experimental arrangement using white light source	5-19
5-13	Spatial distribution of the 4 desired wavelengths	5-21
5-14	Copper encapsulated fibers showing the edge of copper	5-23
5-15	Polished end of fiber array	5-23
5-16	Demultiplexer packaging	5-24
5-17	Wavelength deviations in packaged demultiplexers	5-28

LIST OF TABLES

TABLE		PAGE
4-1	Diffraction Angles of the Four Wavelengths used in the Spectrometer	4-4
4-2	Calculated $\Delta\lambda_{max}$ for Different Waveguide Parameters ($n_2 \cong 1.523$)	4-11
4-3	Calculated $\Delta\lambda_{max}$ as a Function of Waveguide Thickness ($n_2 \cong 1.523$, $n_1 = 1.510$)	4-14
5-1	Waveguide Dimensions and Edge Quality	5-5
5-2	Summary of Waveguide Evaluation	5-8
5-3	Demultiplexer Crosstalk (CT) and Insertion Loss (IL) Characteristics	5-29
6-1	Typical Coupler Characteristics	6-2
6-2	Best Overall Device Characteristics	6-2
6-3	Multiplexer Characteristics	6-3

SECTION 1

INTRODUCTION AND SUMMARY

Fiber optic transmission is emerging as an attractive concept in data distribution on board civil aircraft. Development of an optical data distribution network for Integrated Avionics and control systems for commercial aircraft will provide a data distribution network that gives freedom from EMI and ground loop problems, eliminates crosstalk and short circuits, provides protection and immunity from lightning-induced transients and gives a large bandwidth capability. In addition, there is also the potential for reducing the weight and increasing the reliability over conventional data distribution networks.

Wavelength division multiplexing (WDM) is a candidate method for data communication between the various avionic subsystems. With WDM all systems could conceptually communicate with each other without time sharing and without requiring complicated coding schemes for each computer and subsystem to recognize a message.

Since WDM enables the simultaneous transmission of signals on different optical wavelengths through a single optical fiber, this wavelength diversity also greatly expands the capacity and versatility of future fiber optic links. For instance: (1) each wavelength or optical frequency may be the carrier on which the signals of several users or systems are multiplexed enabling the information carrying capacity of a link to be multiplied by the number of wavelengths used; (2) signals which differ widely in type (e.g., analog and digital), bandwidth or data rate may each be transmitted on a different wavelength allowing a variety of traffic to be carried simultaneously over a single optical fiber; (3) users may couple energy into and out of an existing fiber optic link without requiring access to existing electronic modems.

Part II of this NASA contract program, entitled "Component Development and System Integration," consists of two phases. The objective of Phase I is to develop component technology for the implementation of a wavelength multiplexed data distribution system. The components to be developed include optical couplers for optical wavelength multiplexing, wavelength demultiplexers, and optical connectors. The objective of Phase II is to develop an experimental four-port, four-wavelength data bus for test, evaluation, and demonstration. A schematic of the data bus is shown in Figure 1-1. There are four identical units of demultiplexers, each connected with fiber cables to a 4 x 4 transmission star coupler (multiplexer), which in turn is fed by four transmitters. Each transmitter will emit at a prescribed wavelength.

Our basic design for the demultiplexer is a waveguide version of the Rowland Spectrometer. Under this NASA contract we have fabricated and characterized the device shown schematically in Figure 1-2. The basic structure as shown is a planar optical waveguide with a pair of cylindrical lens-like surfaces. The back surface, upon which a reflection grating is attached, has a radius of curvature, R. The opposite surface, upon which the input and output fibers are attached, is located a distance R away from the grating and has a radius of curvature, R/2. The Rowland geometry is unique in that in the absence of aberration, the optics of the device produce an image of the input spot at the output plane with unity magnification. Furthermore, if a planar waveguide is incorporated into the structure, no external collimating optics are required between the device and the input and output fibers.

The 4 x 4 transmission star coupler was made by flame fusing four fibers together. Trade-offs between optical power distribution uniformity and excess loss were carried along the process. A photo of the completed hardware is shown in Figure 1-3. In the rest of this report we will describe in detail the design, development and characterization of the multipexers, demultiplexer and data bus.

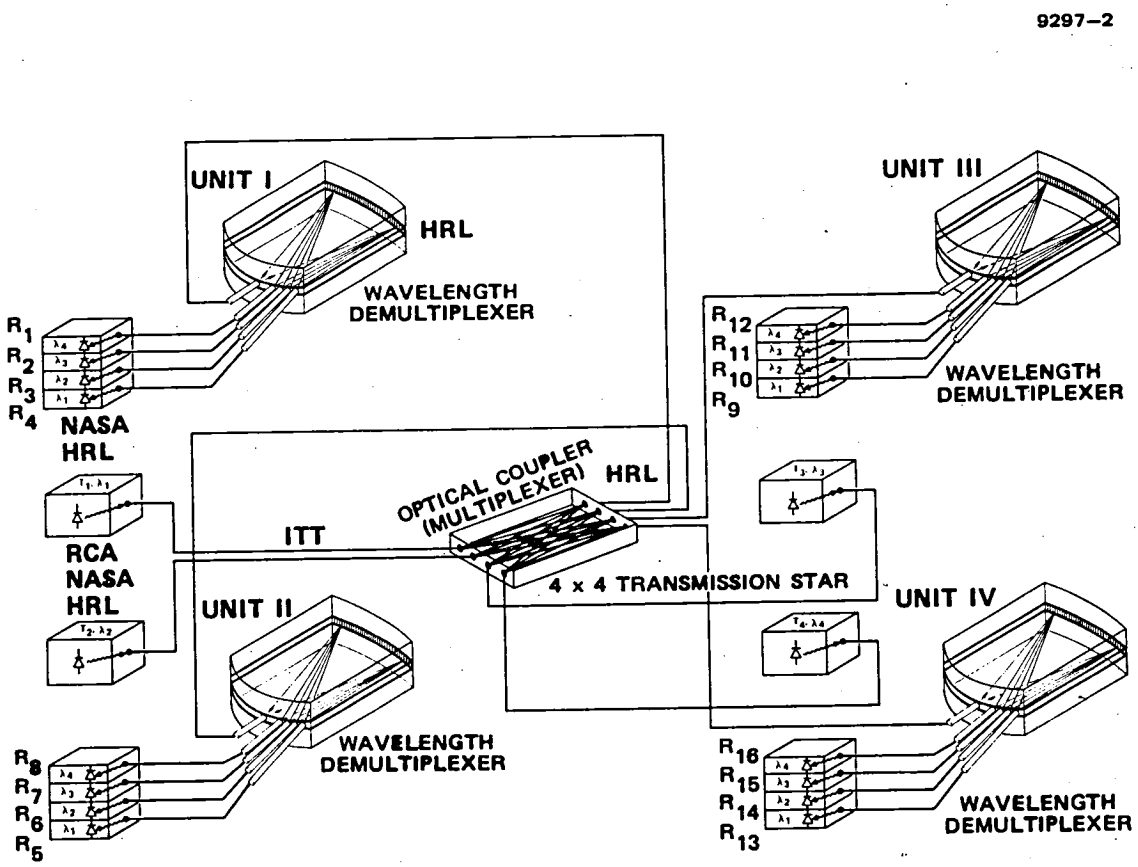

Figure 1-1. Wavelength Multiplexing Data Bus

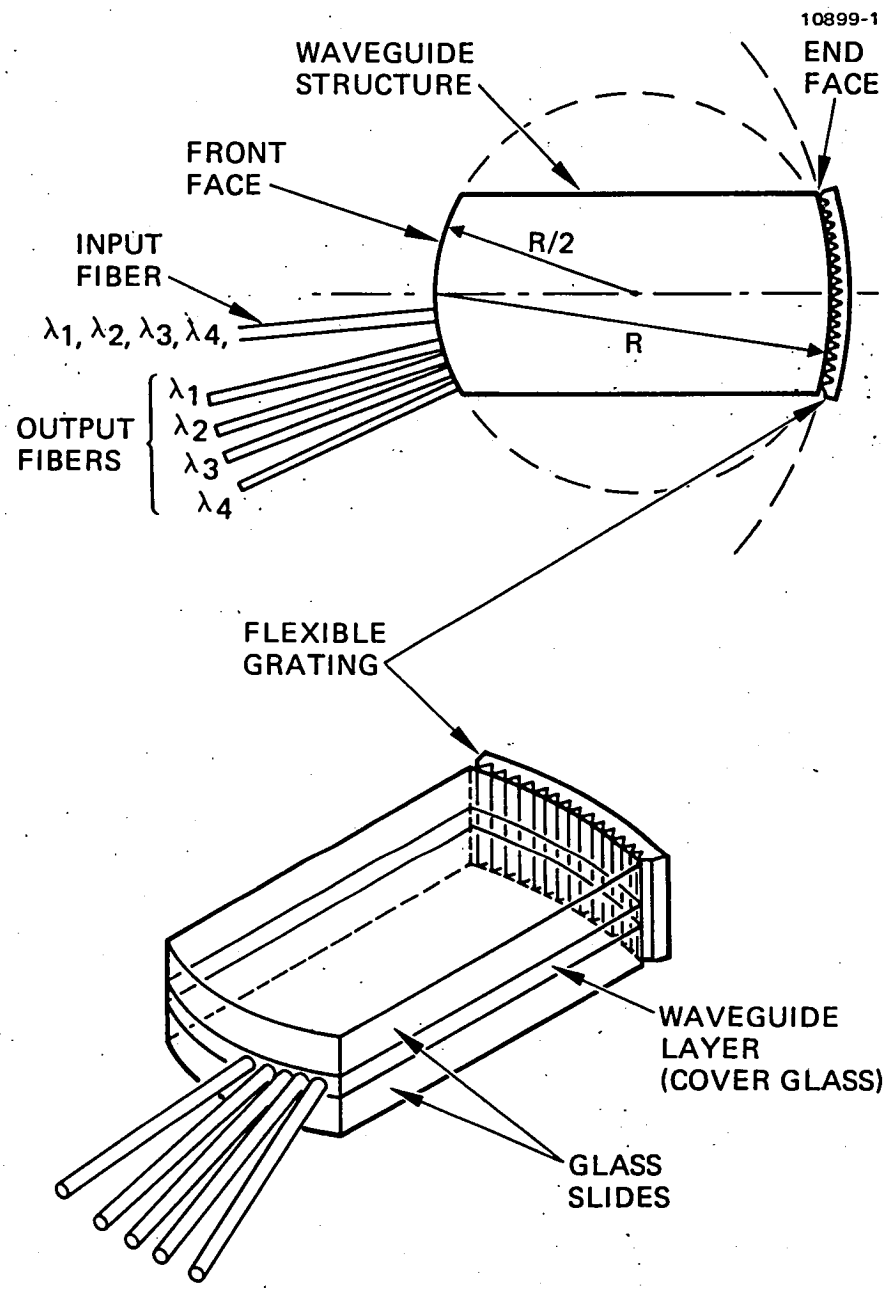

Figure 1-2. Schematic of a planar Rowland Spectrometer.

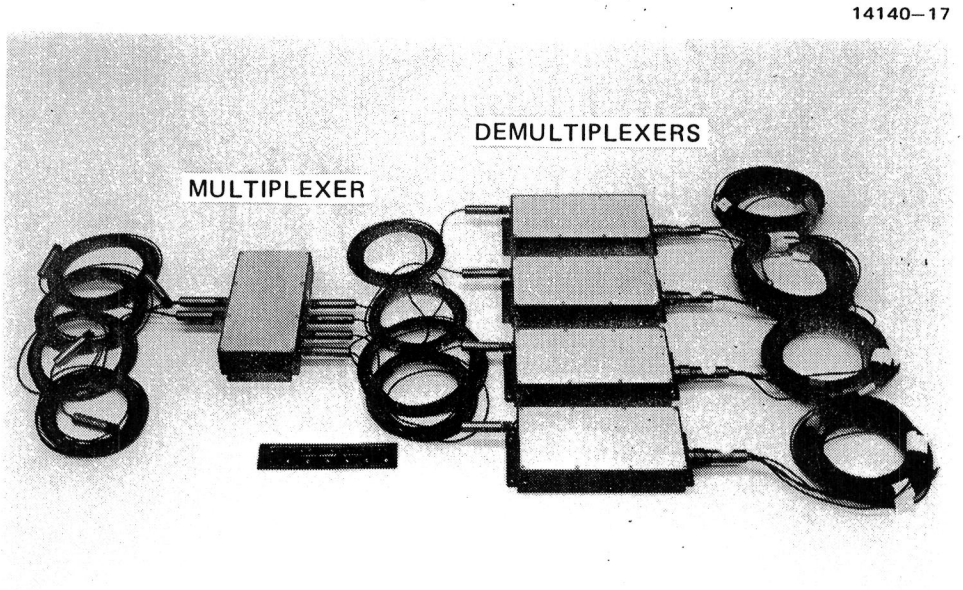

Figure 1-3. The multiplexer and demultiplexers with fiber cable interconnections.

SECTION 2

REVIEW OF WAVELENGTH DIVISION MULTIPLEXING

Recent progress in the manufacture of optical fibers with a wide low-loss spectral window of 0.8 to 1.6 μm and of low-threshold, long-life semiconductor light sources covering the corresponding wavelength region, has made wavelength division multiplexing (WDM) possible. The WDM technique effectively provides multiple transmission channels using a single optical fiber and enables the optical fiber to be used more efficiently. Therefore, this technique is expected to increase the information capacity of a single optical fiber by realizing full duplex transmission of various types of digital and analog modulated signals.

For a WDM system, a multiplexer and a demultiplexer are necessary for the transmitter and the receiver, respectively. A multiplexer consists of input fibers (each coupled to a source of a specific wavelength), a multiplexing circuit, and a transmission fiber. A demultiplexer consists of a transmission fiber, a demultiplexing circuit, and output fibers. A multiplexing circuit couples optical signals of different wavelengths to a single transmission fiber, and a demultiplexer circuit separates these optical multiple signals. Current approaches to optical multiplexing and demultiplexing circuits consist of optical components, such as diffraction gratings, prisms, and thin-film filters. Gratings and prisms are angular dispersive devices, and the filters are wavelength selective devices. There are several publications describing multiplexer designs using these components.[1-5] However, since a demultiplexer design also depends on system requirements including the number of channels, the wavelength region, the type of the optical source, and the optical fiber type, comparisons of demultiplexers using these three basic components are complicated. We will describe some of the techniques that have been proposed or demonstrated for multiplexing and discuss their relative merits with respect to the requirements of this program.

A diagram of a typical WDM system is shown in Figure 2-1(a). It is depicted for single-fiber one-direction transmission. One can easily extend it into two-fiber bidirectional transmission or single-fiber bidirectional transmission by adding additional fiber or wavelengths. These two cases are shown in Figures 2-1(b) and 2-1(c).

In order to avoid unacceptably large insertion loss, it is necessary to use wavelength selective devices based on refractive or interference effects to construct the multiplexer/demultiplexers. All such dispersive devices are also sensitive to the orientation of the input light beam. Thus, to achieve the desired wavelength resolution, the light beam must be collimated to an angular spread smaller than is normally obtained in typical multimode fibers. Therefore, any multiplexer/demultiplexer design must include collimating and focusing optics, and consequently should be considered in the evaluation of the practicality of the design.

A. ANGULAR DISPERSIVE DEVICES

A typical device of this category must have some form of optics to collimate the optical beam from the input fiber. The optical beam must then pass through a wavelength dispersive device, and the output focused back into the output fibers. An important parameter of such a device is the linear dispersion at the output fiber, $dx/d\lambda$. This quantity is, in turn, a function of the angular dispersion of the dispersive element, $d\theta/d\lambda$, and the effective focal length of the optics, f. If optical fibers are used at the output, then a necessary condition for the wavelength separation, $\Delta\lambda$, the fiber output diameter, d, and the device linear dispersion, dx/d, is

$$\frac{dx}{d\lambda} \cdot \Delta\lambda \geq d \quad .$$

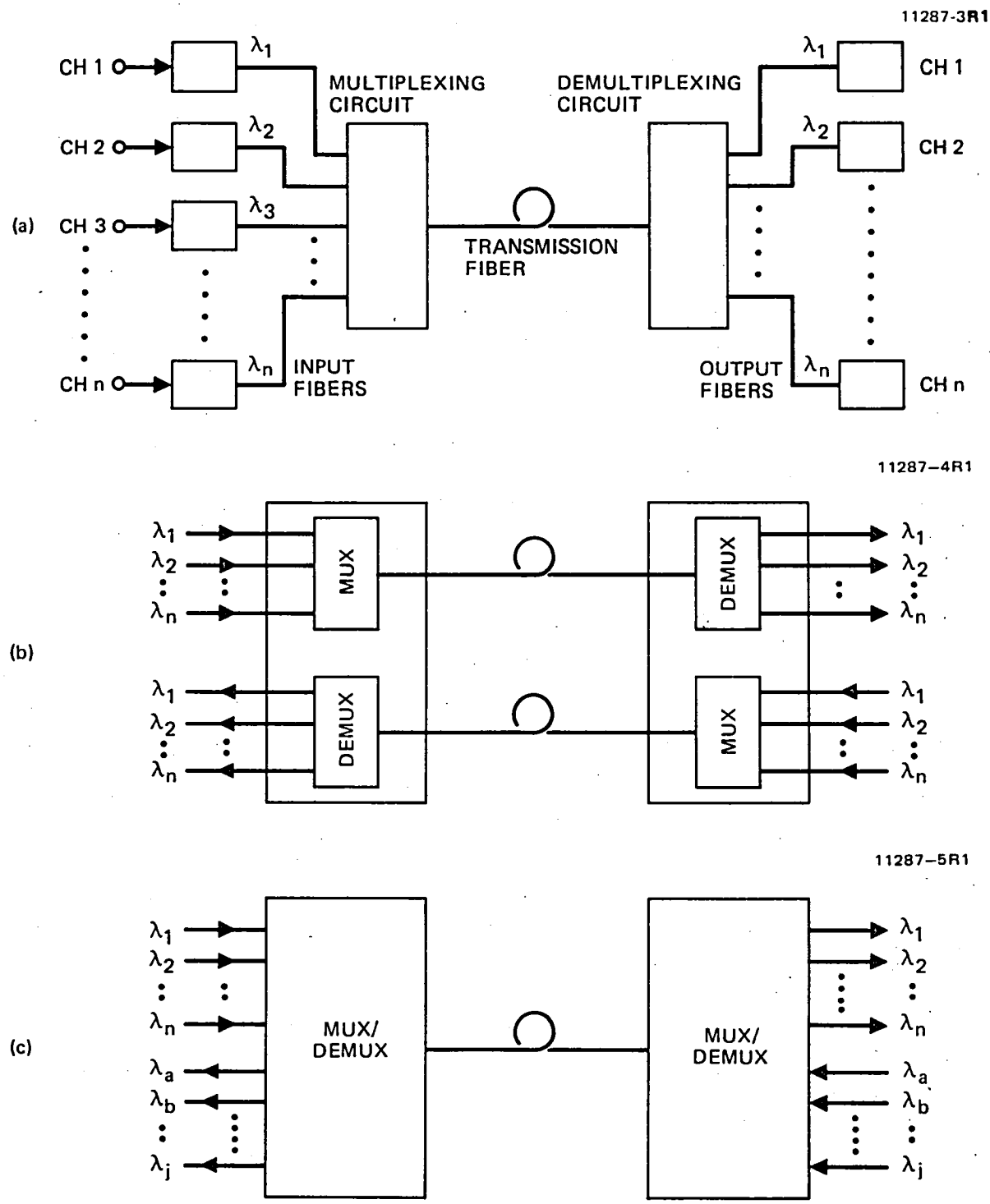

Figure 2-1. Block diagram of a typical wavelength division multiplexing system. (a) Single-fiber one-directional transmission, (b) two-fiber bidirectional transmission, and (c) single-fiber bidirectional transmission.

Furthermore, if the optics have unity magnification, then the intrinsic insertion loss and crosstalk will be zero (for lossless, aberrationless optics with no wavelength error). To use the dispersive device for a multiplexer or demultiplexer it is important to precisely position the input and output fibers; otherwise both insertion loss and crosstalk will increase. For a passive device with identical fibers at the input end and output end, unity magnification from the optics is the optimal situation. Any wavelength deviation or aberration will introduce insertion loss. Crosstalk can usually be made arbitrarily small by using an optic system with large linear dispersion and narrow source line width.

Examples using diffraction gratings as the dispersive element are shown in Figure 2-2. Figure 2-2(a) shows a bulk implementation of a wavelength demultiplexer. With laser diodes as the source this device has been shown to be capable of providing five channels with 200 Å of wavelength separation in the 0.8 - 0.9 μm region and insertion loss of 2-3 dB for 55 μm core input fiber and 100 μm core output fibers. In Figure 2-2(b) another configuration for forming a demultiplexer is shown. Here planar multimode waveguide is employed together with a chirped grating at the back end to partially correct for aberrations. An experimental device of this type used 60-μm core input fibers and 250-μm core output fibers to demonstrate a ten-channel (350 Å separation) demultiplexer in the 1.0 to 1.4 μm wavelength region with insertion loss of ~3 dB and crosstalk isolation of better than 25 dB. Note that both of these examples utilized an output fiber much larger than the input fiber in order to reduce the wavelength sensitivity of the device (i.e., provide a flat pass band for each channel) and to reduce the insertion loss induced by aberrations.

In general diffraction gratings are preferred over prisms at the dispersive element because of their ease in achieving large linear dispersion with a reasonable size device.

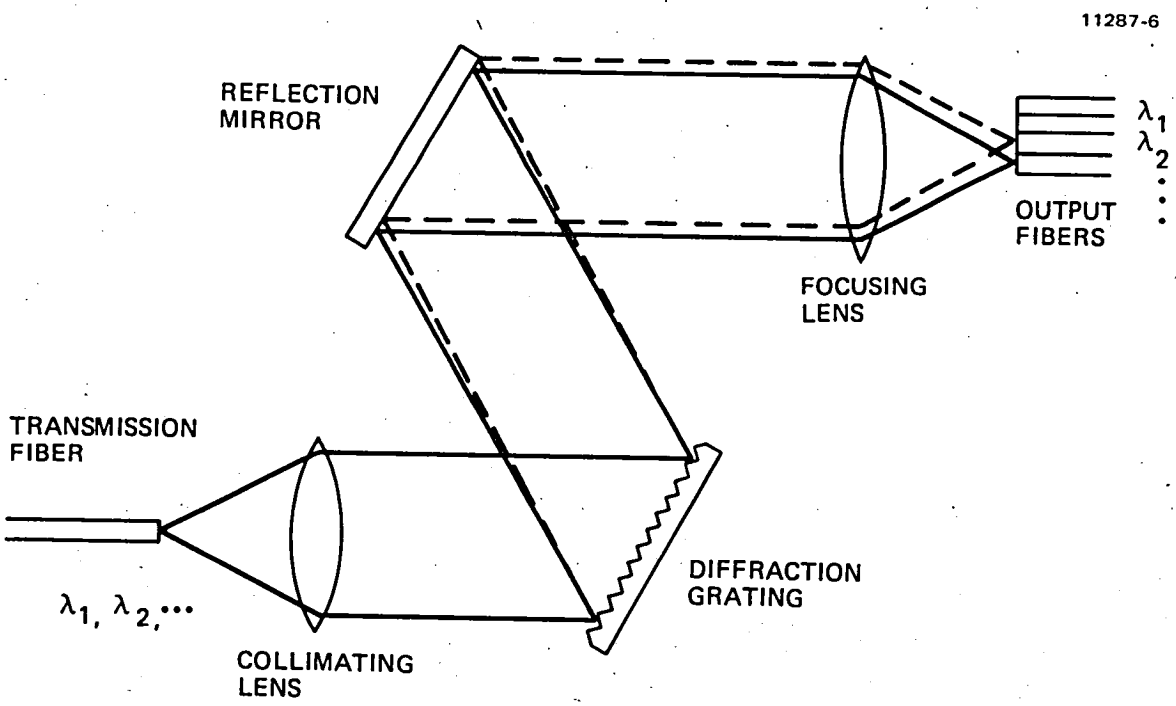

(a) A bulk approach

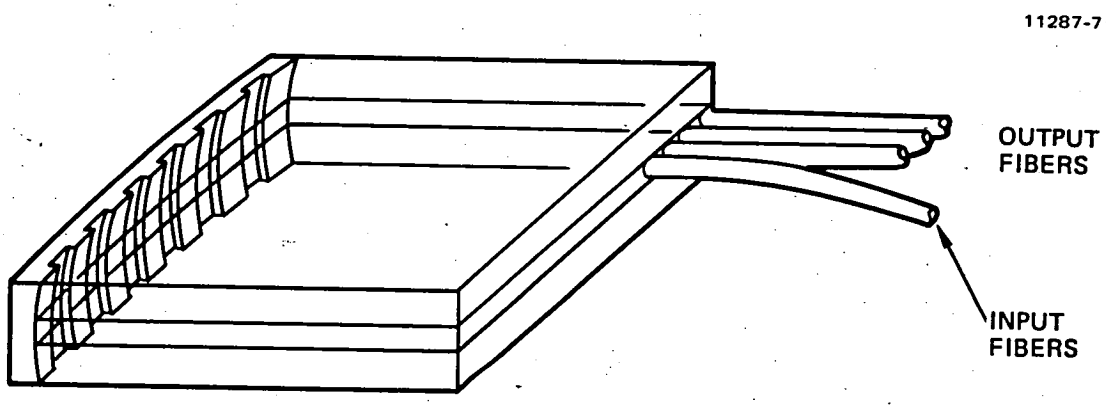

Figure 2-2. Examples of demultiplexers using diffraction gratings. (a) A bulk approach, and (b) a planar approach.

B. INTERFERENCE FILTERS

Typical interference filters consist of a multilayer structure of two different materials (with different indices of refraction). The arrangement of the layer structures dictates the resultant spectral characteristics. These filters can be designed as either short-wavelength pass filters, long-wavelength pass filters, or band pass filters. Compared to the diffraction grating approach, a multiplexer/demultiplexer made of interference filters tends to have higher crosstalk but is relatively insensitive to wavelength errors. The effects of incident beam polarization must be taken into account if the incident angle is other than 90°. Two examples of a multiplexer/demultiplexer using interference filters are shown in Figure 2-3. Figure 2-3(a) shows a very simple device for two-channel application. Fiber number 1 contains two wavelengths, λ_1 and λ_2, incident on a graded index rod lens. The end of the lens rod is equipped with an interference filter that reflects λ_1 and transmits λ_2. Outside of the rod lens is a reflection mirror slightly tilted with respect to the lens end, such that the reflected signal at λ_2 is focused back into Fiber 3. The advantage of this device is that it has relatively low insertion loss and is quite compact. However, it is difficult to extend this dichroic concept to a multi-channel device structure. Figure 2-3(b) shows a structure for a multireflection multi/demultiplexer. Each filter shown has a different central pass band frequency; therefore, upon successive reflections different wavelengths are dropped off into their respective channels. One such device has been characterized as a 6-channel demultiplexer with insertion loss per channel around 1 dB. However, the crosstalk level in this device is greater than -20 dB for channel separations of 400 Å.

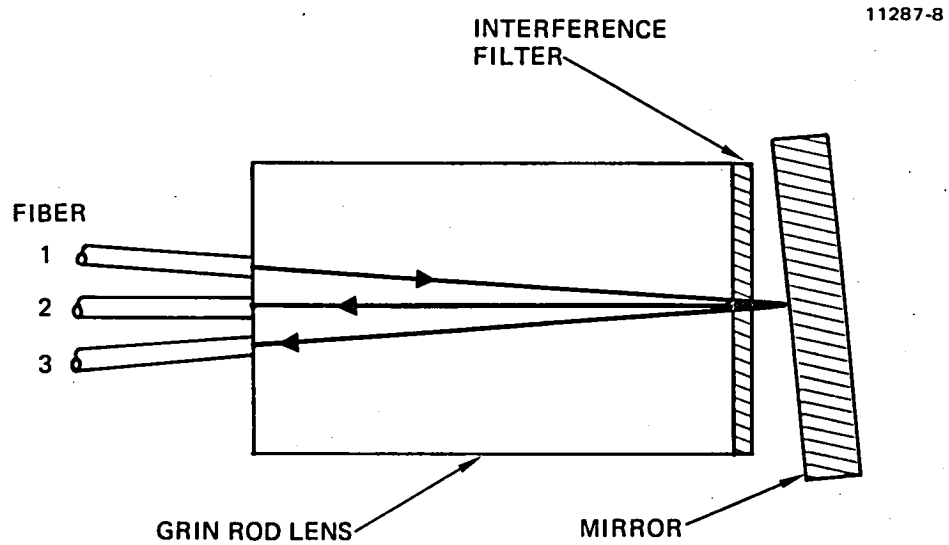

(a) A simple two-channel decoupler

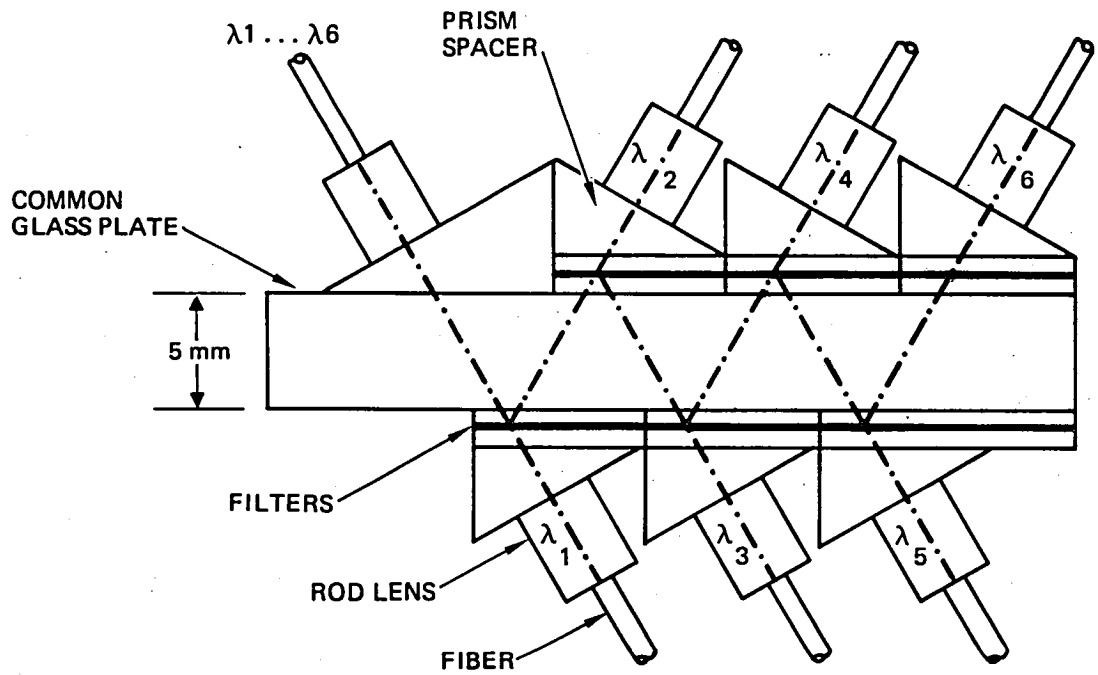

Figure 2-3. Examples of demultiplexers using interference filters. (a) A simple two-channel decoupler. (b) A multi-channel multiplexer-demultiplexer.

To summarize this subsection, we have shown that there are no fundamental limitations to the fabrication of passive wavelength multiplexers which are compatible with the characteristics and requirements of some of the proposed fiber optic transmission systems; however, there are significant differences between the various devices. We agree with the results of a study carried out by W.J. Tomlinson [1] who indicates that the blazed grating device is currently superior to all the other devices that he considered. The blazed grating requires only a small number of components, is relatively insensitive to polarization, and has low crosstalk. In contrast, interference filters tend to have higher crosstalk, are strongly polarization dependent and must have greater channel spacings. In the next subsection we will describe the development of a unique demultiplexer structure based on a blazed grating technique under this contract program.

SECTION 3

PLANAR ROWLAND SPECTROMETER AS A DEMULTIPLEXER

As we have discussed earlier, a number of wavelength demultiplexers have been constructed using a plane grating and GRIN-rod lens. These devices are small and rugged; however, these so-called 3-dimensional micro-optics devices require lenses and precise 3-D adjustment of input and output fibers in the focal plane. As an alternate two-dimensional approach, multimode slab waveguides have been introduced as the basic structure for multiplexer/demultiplexers.[5,6] In this section we describe the design, fabrication, and characterization of a planar Rowland Spectrometer[7] as a demultiplexer.

A. PRINCIPLE OF OPERATION

The geometry of the Rowland device is shown in Figure 1-2. The basic structure is a planar optical waveguide with a pair of cylindrical surfaces. The back surface, upon which a reflection grating is attached, has a radius of curvature R. The opposite surface, upon which the input and output fibers are attached, is located a distance R away from the grating and has a radius of curvature R/2. In Figure 3-1, assume that a point source C emits light that is confined to a plane and covers an angle $\angle ACB$. Using a geometrical argument, the ray CA incident on the grating at point A sees an incident angle $\angle OAC$ (since OA is the normal to the grating surface at A). The ray CA will be diffracted and becomes ray AD according to the grating equation:

$$\sin(\angle OAC) + \sin(\angle OAD) = \frac{m\lambda}{nd} , \qquad (1)$$

11287-9

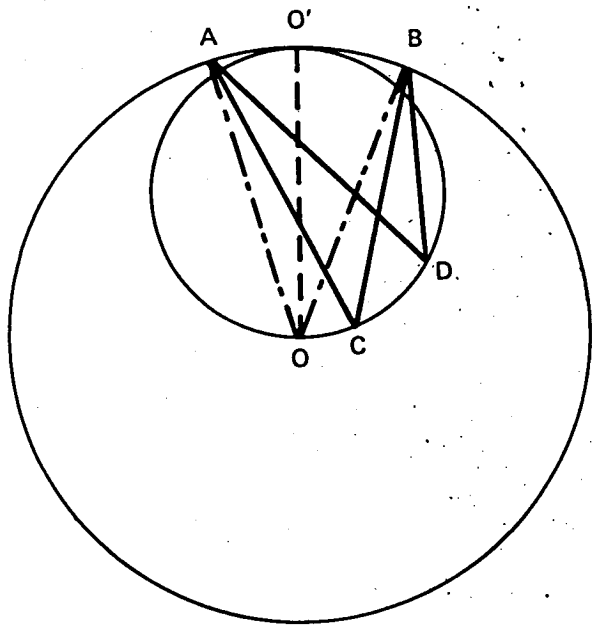

Figure 3-1. Illustration of the Rowland circle principle.

where m is the diffraction order, λ is the wavelength, n is the index of refraction of the medium, and d is the grating constant. Now consider a second ray, CB with an incident angle at point B of $\angle OBC$. If both A and B are not too far away from the tangent point of the two circles at 0', then both A and B can be approximated as being on the small circle as well as on the larger one. As a result we have

$$\angle OAC \approx \angle OBC \quad ; \tag{2}$$

thus, the diffracted ray from point B will also pass through D, since from equations (1) and (2) we must have

$$\angle CAD \approx \angle CBD \quad . \tag{3}$$

Likewise for ray CO', the diffracted ray is O'D. Thus we conclude that a structure as shown in Figure 1-2 can diffract and focus a diverging light source at point C to point D on the small circle. Since the output from a multimode fiber resembles that of a diverging point source, it is reasonable to expect that an image of the input fiber (located at C) will appear at point D. From geometric optics, the structure is a one-to-one imaging system. However, because of aberration, diffraction and grating imperfection, the image will be distorted.

In the discussions above, we condisdered only one-dimensional imaging. In reality, the output of a multimode fiber diverges in two dimensions. By incorporating a planar waveguide structure into the device, however, we can confine the fiber output in the vertical direction and have a situation which resembles the one-dimensional case just discussed. Therefore, a planar Rowland Spectrometer combines the operation of a diffraction grating with a concave mirror to achieve spectral point-to-point imaging. It is potentially rugged and does not require any additional focusing or collimating optics.

The demultiplexer is designed to operate in the wavelength region of 0.8 to 0.86 μm using commercially availble GaAs/GaAlAs injection lasers. The wavelength separation between channels in the system is 100 Å, and four channels are required.

B. FIRST GENERATION DEVICES

Glass waveguides formed by epoxying a thin cover glass (~75 μm thick) in between two microscope slides were used. The waveguide is 5.08 cm long and 2.54 cm wide. The two end faces of the waveguide were polished to have radii of curvature of 2.54 cm (front face) and 5.08 cm (back face), respectively. In actual fabrication 30 demultiplexer structures are polished together as one piece. The tolerance on the various dimensions is chosen to be ±25 μm to avoid severe defocusing and aberration of the output spot. The period of the reflection grating was chosen to be 2 μm, which for an incident angle of 5° gives a diffraction angle in the range of 10.1° to 11.3° when the wavelength varies from 0.8 μm to 0.86 μm. The input optical signal which contains multiple wavelengths (channels) is coupled to the spectrometer through a graded-index fiber (~55 μm core). In the waveguide plane the optical beam diffracts according to the effective numerical aperture of the input fiber relative to glass; in the vertical direction it is confined by the waveguide structure. Upon diffraction by the grating, the wavelength components of the beam are separated and focused (due to the waveguide end face curvature) into different spots along the front face of the spectrometer. For each wavelength position, there will be a fiber (100 μm core) to collect the output signal. The larger core size of the output fiber is to reduce the channel insertion loss caused by aberration.

In our initial experiments a commercial plastic replica grating was used. The results were not satisfactory because the grating surface was distorted through the handling process. This grating distortion in turn generates severe image aberration at

the output. It was recognized that a semirigid grating substrate is necessary to minimize the effects of handling. Therefore, we fabricated several diffraction gratings on thin glass substrates (~75 μm thick) using a holographic exposure and ion beam etching process. The grating thus fabricated showed good quality and uniformity. The overall diffraction efficiency (all orders) was better than 90%; however, depending on the groove depth, the diffraction efficiency for the desired order (m = -1) was no more than 40%. The gratings were inserted in a fixture that had a contoured back piece to force the grating to conform to the shape of the spectrometer. It was found that if the grating curvature deviates from that of the waveguide, a defocused (or aberrated) output spot will result.

Experimental characterizations of the demultiplexer were carried out using both He-Ne lasers and GaAs-GaAlAs lasers. The laser output was coupled to the spectrometer via a 55 μm core graded-index fiber. The spectrometer output spot size was measured by scanning a 4.5 μm core single-mode fiber across the output face and the collected optical power was recorded as a function of fiber displacement. Figure 3-2(a) shows one such plot for a He-Ne laser ($\lambda = 0.6328$ μm) and Figure 3-2(b) is a similar plot for a GaAlAs laser (single longitudinal mode $\lambda = 0.8255$ μm). These plots are characterized by a relatively sharp peak with a broad base. For the He-Ne laser, the base is about 100 μm wide and for the GaAlAs laser, the base is about 110 μm wide. These values are far greater than the input spot size 60 μm. This is due partially to the intrinsic aberration of the Rowland geometry and partially to the multimode waveguide dispersion. The larger the input fiber numerical aperture (N.A.), the larger the output image aberration will be. This is evident by comparing the He-Ne laser response to that of the GaAlAs laser. Although both signals were coupled into the 55 μm core fiber initially, the fiber N.A. was not filled in the He-Ne laser case,

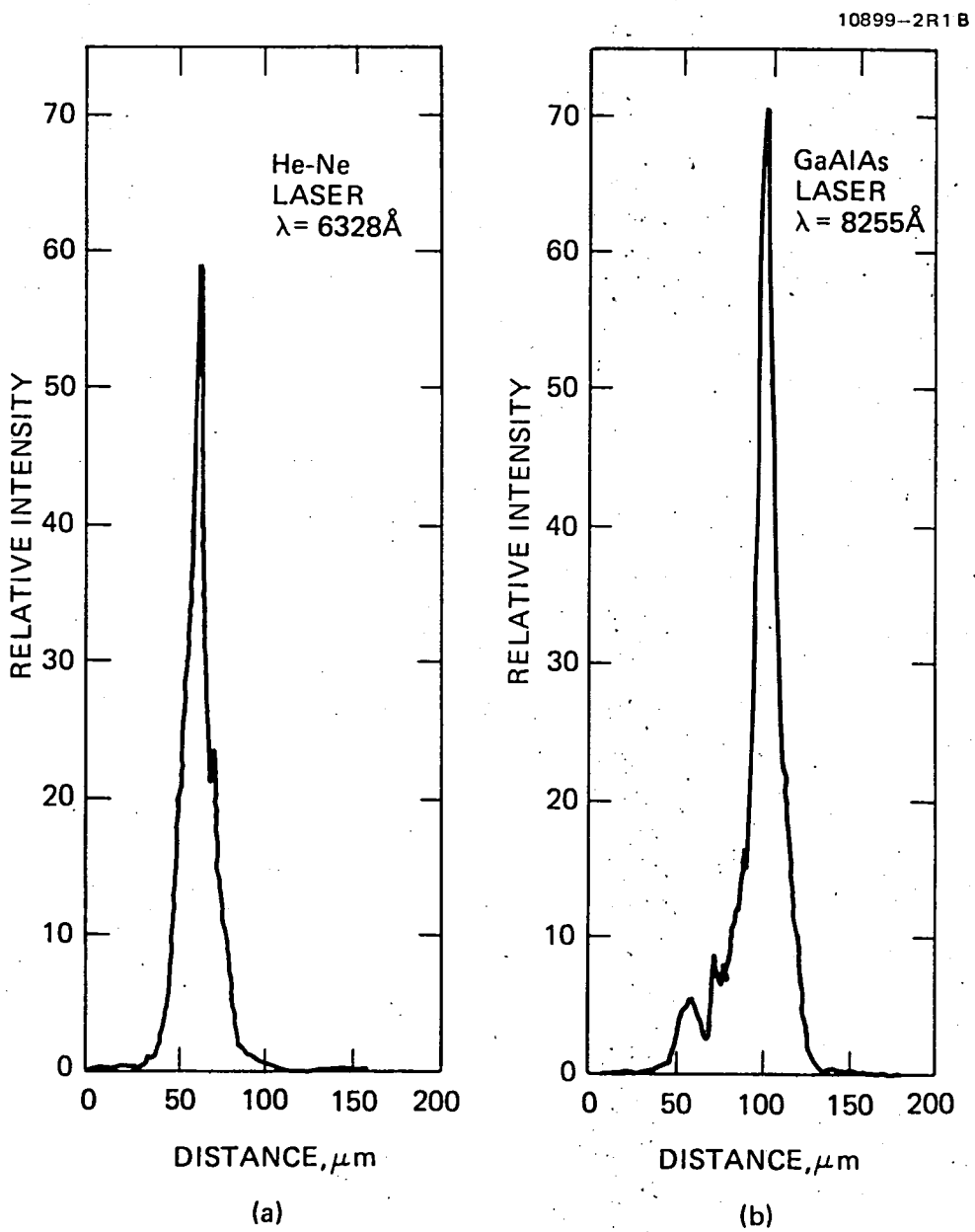

Figure 3-2. Intensity profile at the output face with 55 μm core input fiber excitation (a) using He-Ne laser, λ = 6328 Å. (b) using semiconductor laser, λ = 8255 Å.

while in the GaAs laser case, the fiber N.A. was completely filled. Therefore, the 0.8255 μm radiation illuminated a larger width of the grating and hence suffered more severe aberration.

Likewise, we have used a 100 μm core multimode fiber to scan the output spot rather than using a single-mode fiber. Then the optical power collected as a function of the fiber position does not yield the output spot size, but rather provides information on where the optimal output fiber position is for a given input wavelength. This scan also reveals how much optical power is collected by the output fiber at any given position. This information can be used to determine the crosstalk levels in adjacent fibers (channels) of the demultiplexer.

Several experiments were carried out using two wavelength input signals. The experimental arrangement is shown in Figure 3-3. Two semiconductor lasers were coupled to the input ports of 2 x 2 fused fiber star-coupler. One of the output ports was fed to a detector for power monitoring; the other output port was butt-coupled to the input fiber of the spectrometer. At the output of the spectrometer a 100 μm core fiber was scanned as described above, and the optical power was recorded as a function of fiber position. Figure 3-4(a) shows one such two-wavelength scan. One of the lasers was single mode with $\lambda = 8255$ Å; the other laser was multimode with center wavelength around 8445 Å. The two peaks in the graph are separated in position by 330 μm and by ~190 Å in wavelength, corresponding to a device wavelength dispersion of ~1.74 μm/Å. We have also superimposed on the plot two curves taken with one laser on at a time. From these curves we estimated the cross talk in this case to be greater than -20 dB at both channel positions. Figure 3-4(b) shows a similar plot, but for two lasers with center wavelengths of 8312 Å and 8410 Å. the crosstalk level at each channel location is -18 dB and -14 dB respectively. The reason for the nonsymmetrical crosstalk level is that the 8410 Å laser has a full width half

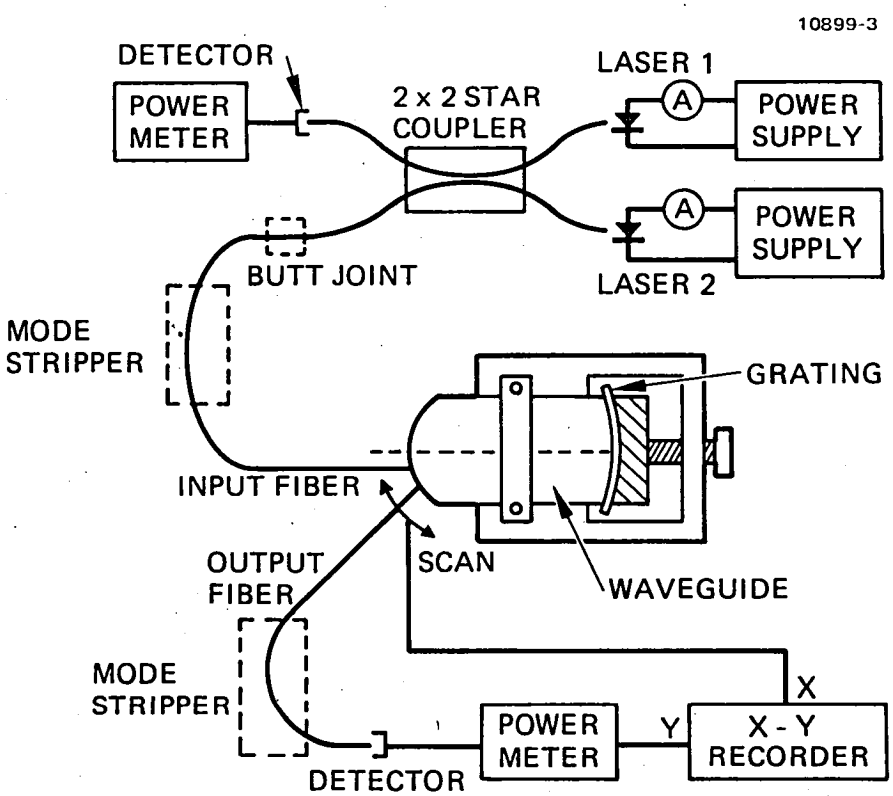

Figure 3-3. Experimental arrangement for demultiplexer characterization.

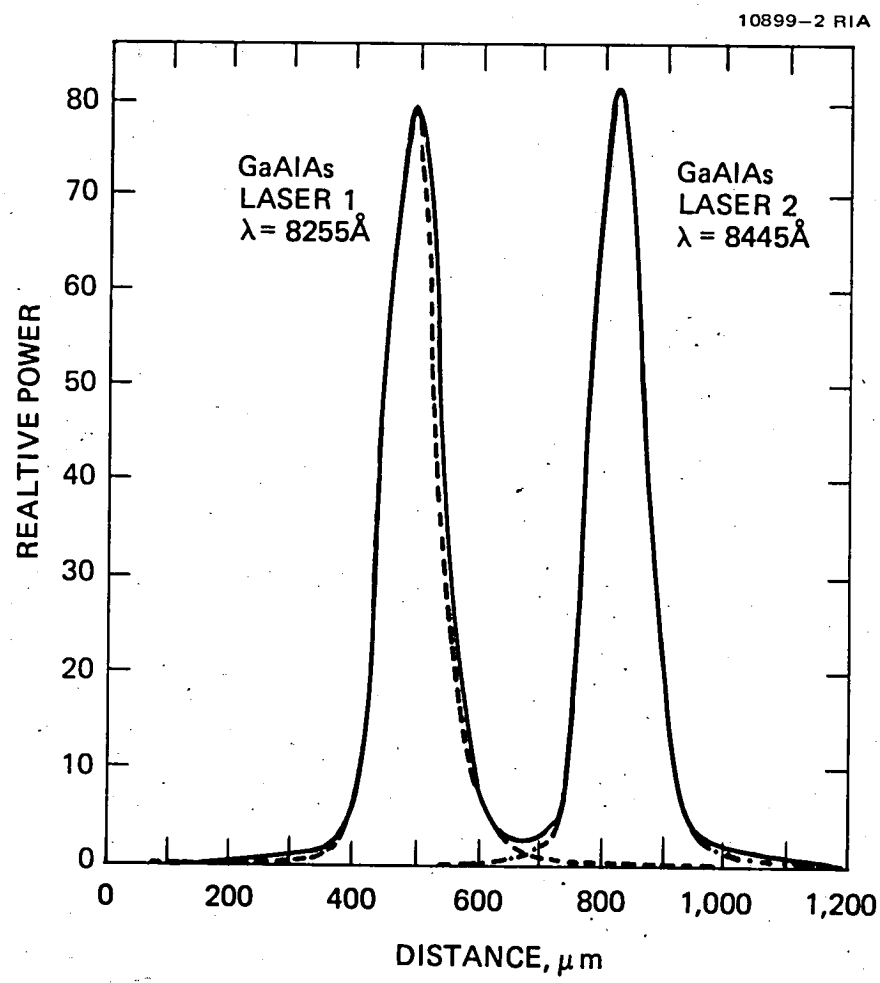

Figure 3-4(a). Demultiplexer output as a function of output fiber position. The solid curves were taken with both lasers on simultaneously; the broken curves were taken with one laser on at a time. The two peaks correspond to λ = 8255 Å and λ = 8455 Å.

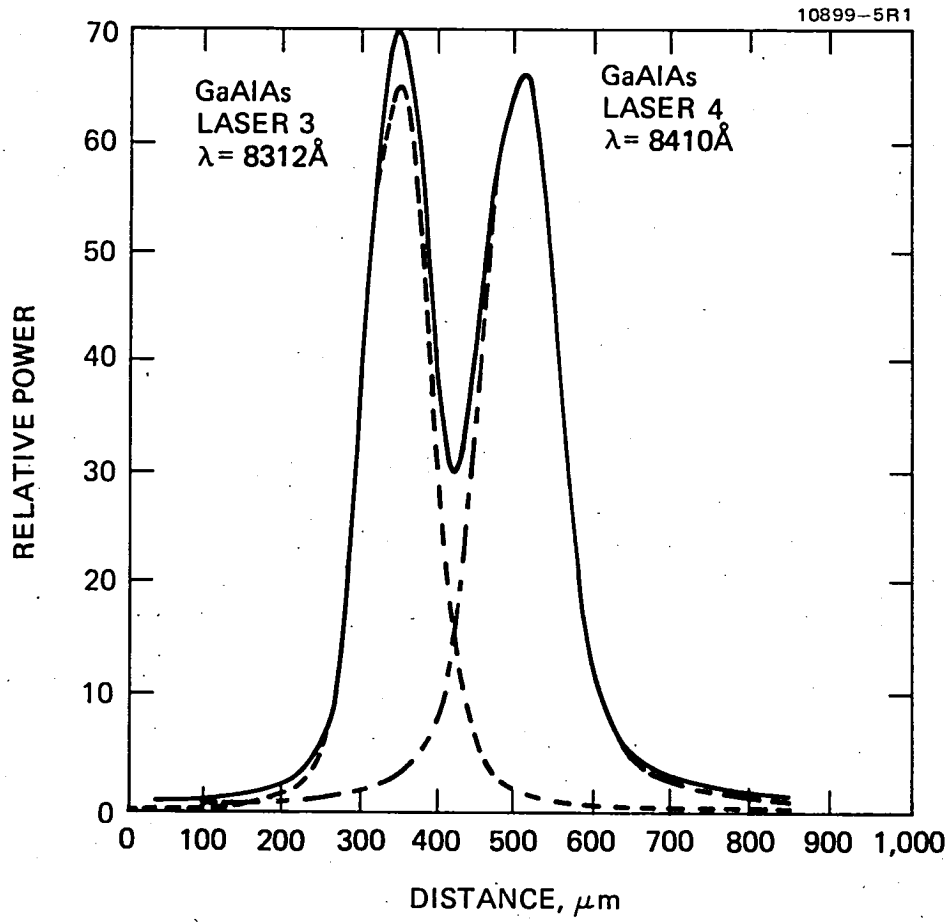

Figure 3-4(b). Demultiplexer output as a function of output fiber position. The solid curves were taken with both lasers on simultaneously; the broken curves were taken with one laser on at a time. (b) The two peaks correspond to λ = 8312 Å and λ = 8410 Å.

maximum spectral width of 20 Å while that of the 8312 Å laser is only ~12 Å. Typical insertion loss per channel, measured as the ratio of the output fiber optical power to that of the input fiber was ~9 dB. More than half of that is due to the poor grating diffraction efficiency (-5 dB). We can attribute about 3 dB to the waveguide propagation loss and the remaining 1 dB loss to waveguide-to-fiber coupling.

In summary, we have shown that a planar Rowland geometry spectrometer can be used as a high channel density wavelength demultiplexer with crosstalk isolation approaching 20 dB for two channels separated by 175 μm (output fibers center-to-center distance) and with 100 Å wavelength difference. Although the insertion loss and the output spot aberration are quite large in our present prototype, better results could be obtained with the following improvements:

- Use semiconductor lasers with narrow spectral width and low spontaneous emission level to reduce channel crosstalk and to increase through-put efficiency.

- Use a blazed grating to increase the diffraction efficiency into the desired order (m = -1).

- Use a chirped grating instead of a constant period grating to reduce intrinsic device aberration. It can be shown that if the grating spacing is periodic on a chord (parallel to the tangent through the apex of the waveguide), the device aberration is minimized.[8]

- Use modified waveguide structures to reduce the multimode waveguide dispersion effect. The waveguide dispersion leads to waveguide modes propagating with a range of effective mode index. Thus the modes of the waveguide upon incidence on the grating will be diffracted in various directions even though they have identical incident angle. One solution under investigation is to use a waveguide with an expanding taper.

- Use ion-exchange or CVD process for waveguide formation to reduce scattering loss from air bubbles in the epoxy.

SECTION 4

IMPROVED DEMULTIPLEXER DESIGN

Based on the results discussed in the the last section, we decided to use improved planar Rowland spectrometers as the demultiplexers in the final deliverables.

The basic building block of our demultiplexer is shown in Figure 4-1. The differences between this device and that shown in Figure 1-2 are: (1) a rigid, ruled grating (properly blazed) is used rather than a flexible one; (2) a tapered waveguide layer is used rather than one with uniform thickness; and (3) the grating is ruled with periodic spacing on a chord parallel to the tangent through the apex of the waveguide rather than with equal spacing along the arc. These modifications are expected to greatly improve the device performance over that presented in Section 3B.

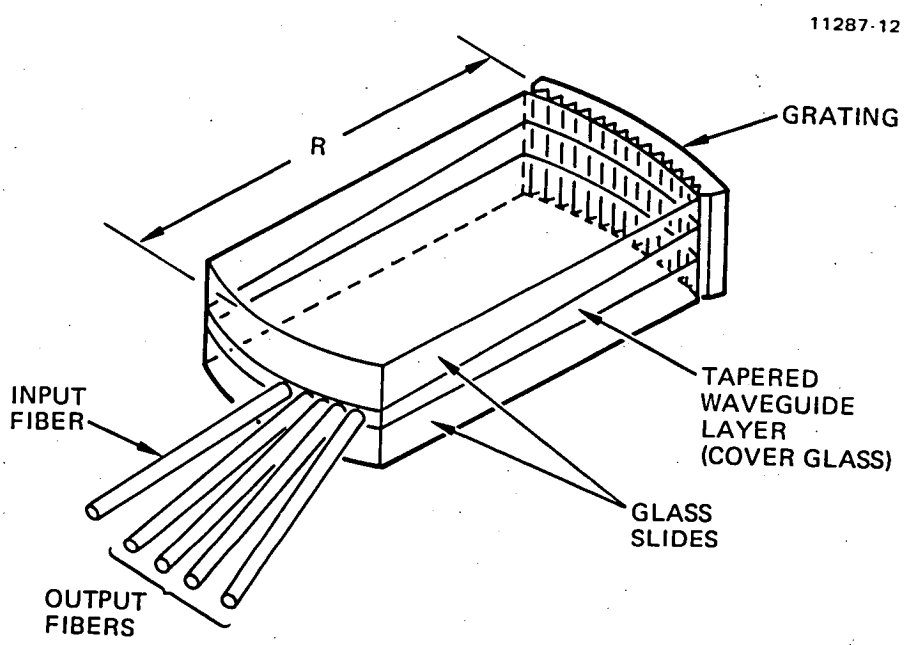

Figure 4-1. Planar Rowland spectrometer with modified structure.

A. DEVICE DESIGN

The planar construction is chosen because of the structural ruggedness. Rowland circle geometry is adopted because no additional collimating or focusing optics is required. In comparison, lenses or GRIN rods are sensitive to wavelength variations and therefore will affect the insertion loss and cross talk of the device. Diffraction grating is used because of its achievable large dispersion and high crosstalk isolations with reasonable device size. It is also relatively insensitive to incident optical polarizations compared with filter devices. The most critical issue of this device, however, is the wavelength sensitivity of the insertion loss.

Any laser wavelength drift will result in increased insertion loss and perhaps even crosstalk level.

The basic design equation for the device is

$$\sin\alpha + \sin\beta = \frac{\lambda}{nd} \quad , \tag{4}$$

where α is the incident angle, β is the diffraction angle, λ/n is the optical wavelength in the waveguide and d is the grating period. The angular dispersion of the grating is given by

$$\frac{d\beta}{d\lambda} = \frac{1}{n\ d\ \cos\beta} , \tag{5}$$

for a fixed incident angle α.

From Figure 4-1, the linear dispersion of the device is roughly given by $R \cdot (d\beta/d\lambda)$. Thus for two channels with wavelength separation of $\Delta\lambda$, the diffracted output spots will be separated by

$$\Delta L = R \cdot \frac{d\beta}{d\lambda} \Delta\lambda = \frac{R\Delta\lambda}{n\ d\ \cos\beta} \quad . \tag{6}$$

The parameters R, $\Delta\lambda$ and d are chosen such that ΔL is greater than one fiber outer diameter, 125 μm. Also d is chosen such that the device can operate at 0.8-0.86 μm region.

We have selected R = 7.6 μm, d = 1.6 μm, and $\Delta\lambda$= 100 Å as our initial design. The input incident angle is chosen to be α = 6°. Four GaAs lasers with wavelengths of 0.8050 μm, 0.8150 μm, 0.8250 μm, and 0.8350 μm will be used for the system. These wavelengths are chosen based on their commercial availability.

Figure 4-2 illustrates the relation between the incident rays and the diffracted rays. The maximum diffracted angle β_{max} for a device that is 7.6 cm long and 4.0 cm wide is about 14 degrees. Table 4-1 lists the various diffraction angles for the eight wavelengths to be used.

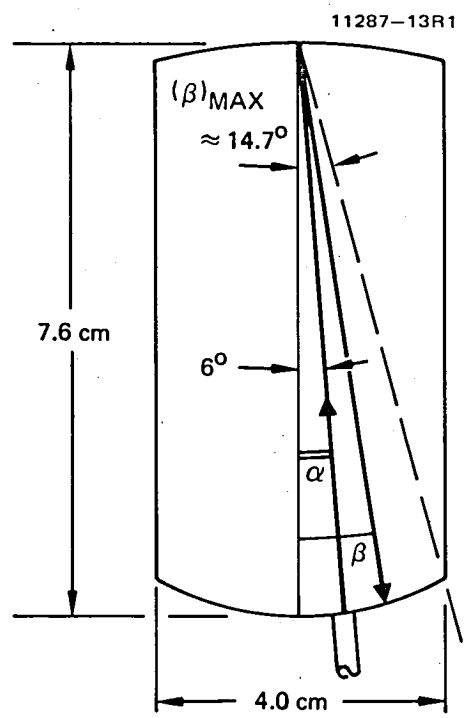

Figure 4-2. Relation between the incident angle α and the diffracted angle β.

Table 4-1. Diffraction Angles of the Four Wavelengths used in the Spectrometer. ($\alpha = 6°$, $d = 1.6\ \mu m$, $n = 1.523$, $R = 7.60$ cm)

Wavelength, μm	0.805	0.815	0.825	0.835
β, degree	13.05	13.29	13.53	13.78
$\Delta\lambda$, Å	100	100	100	
Linear Separation, μm	318	318	331	
Linear Dispersion, μm/Å	3.18			

It is obvious that the Rowland spectrometer can be designed to have even higher channel density by using larger device length and width and smaller grating constant.

B. ABERRATION OF THE DEVICE

In Figure 4-3, consider a point source located at C and follow two rays eminent from C, CA and CB. OA and OB are the local normals to the grating surface at points A and B, respectively. From simple geometry

$$\angle OBC = \angle OFC = \angle OAC + \angle AOF,$$

therefore $\angle OBC > \angle OAC$, or $\alpha_o > \alpha$.
At both A and B, the grating equation should hold; i.e.,

$$\sin \alpha_o + \sin \beta_o = \frac{\lambda}{nd}$$

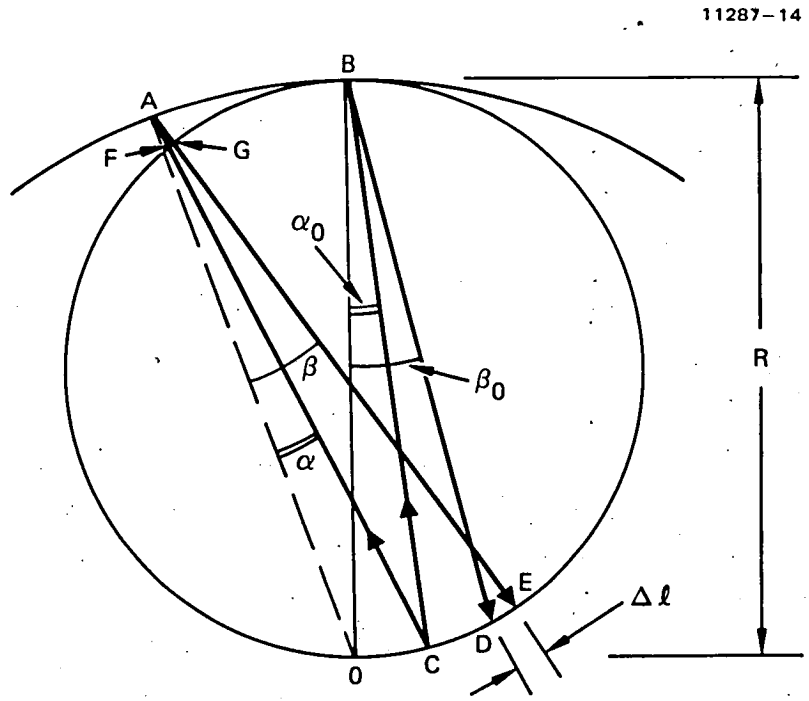

Figure 4-3. Geometrical illustration of the inherent aberration associated with a Rowland spectrometer.

and

$$\sin\alpha + \sin\beta = \frac{\lambda}{nd}$$

where d_o and d are the grating constants at B and A, respectively. If a constant spacing grating is used, $d_o = d$. Since $\alpha_o > \alpha$, it follows that $\beta > \beta_o$.

Furthermore

$$\angle OGE = \beta + \angle AOG,$$

therefore

$$\widehat{OE} > \widehat{OD}$$

and the difference $\Delta\ell = \widehat{DE}$ is the linear aberration of a point source at the output plane. We can estimate $\Delta\ell$ using simple geometrical arguments. Let $\alpha_o = \alpha + \Delta$ and $\angle AOB = \phi$

where

$$\Delta \doteqdot \frac{R(1-\cos\phi)\alpha}{R\cos\phi} = \left(\frac{1}{\cos\phi} - 1\right)\alpha$$

thus

$$\alpha + \Delta = \alpha_o = \frac{\alpha}{\cos\phi}$$

or

$$\alpha = \alpha_o \cos\phi \ . \tag{7}$$

Let $\angle OGE = \Theta$, then the diffracted angle $\beta = \Theta - \delta$

or

$$\Theta = \beta + \delta \doteqdot \beta + \Delta\frac{\beta}{\alpha} \tag{8}$$

Therefore

$$\Delta\ell = R(\Theta - \beta_o) = R(\beta + \Delta\frac{\beta}{\alpha} - \beta_o)$$

$$= R\left(\beta + \frac{1 - \cos\phi}{\cos\phi}\beta - \beta_o\right) = R\left(\frac{\beta}{\cos\phi} - \beta_0\right) \tag{9}$$

This is the inherent aberration of the Rowland Spectrometer if a constant period grating is used. As a numerical example, for $\alpha = 6.0°$, $R = 7.6$ cm, $d = 1.6$ μm, $n = 1.523$, $\lambda = 0.835$ μm and $\phi = 8.05°$, we have $\Delta\ell = 262$ μm. That is, a point source will be imaged into a line of approximately 262 μm long at the output face of the spectrometer.

To minimize the aberration, we can return to equation (9) and set $\Delta\ell = 0$, which requires that $\beta = \beta_o \cos\phi$. For small angles,

$$\alpha_o \doteqdot \sin\alpha_o, \quad \beta_o \doteqdot \sin\beta_o$$

$$\alpha \doteqdot \sin\alpha, \quad \beta \doteqdot \sin\beta \quad .$$

Therefore, using equations (4) and (7) we have

$$\alpha_o + \beta_o = \frac{\lambda}{nd_o} = \frac{1}{\cos\phi}(\alpha + \beta)$$

and

$$\alpha + \beta = \frac{\lambda}{nd} \; .$$

Thus, to minimize $\Delta\ell$ we must have

$$d = \frac{d_o}{\cos\phi} \tag{10}$$

This condition is met if a curved grating is ruled such that the spacing is constant (d_o) along the chord parallel to the tangent of the apex as shown in Figure 4-4. Let's go back to the previous numerical example. With identical parameters except for using a chirped grating, we find that $\Delta\ell = 3.8$ μm (compared with 262 μm for the equally spaced grating).

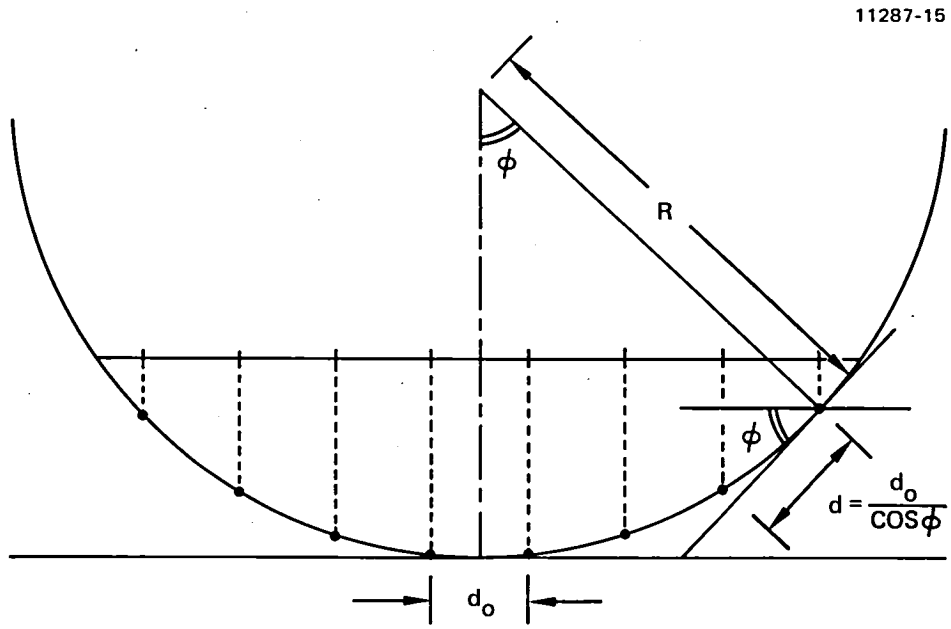

Figure 4-4. The condition for minimum aberration is that the grating period along the arc varies as $d = d_o/\cos\varphi$.

Although the above calculations are based on geometrical argument they have been shown to agree well with computer plots of the device response. As a matter of fact, if the grating spacing is corrected as stated above, near diffraction limited performance is achievable with the spectrometer.

To fabricate such a grating is straightforward. It can be done by direct ruling on the backside of the waveguide, or, more practically, by ruling on a separate matching back piece and then permanently fixing to the waveguide structure.

C. WAVEGUIDE DISPERSION

The slab waveguide used in our previous spectrometer consists of a guiding layer with index of 1.523 and thickness of 75 μm

surrounded by a medium with index of 1.510. At $\lambda = 0.83\ \mu m$ this waveguide can support 36 guided TE modes and same number of TM modes. When excited by the input fiber, the fields in the waveguide can be viewed as composed of slab waveguide modes propagating in a range of angles corresponding to the N.A. of the fiber with respect to glass. Along each propagation direction there exists transverse modes (with mode number m) there is an associated propagation constant k_m. The ratio of k_m and k_o, the free space propagation constant of the wave, defines and effective mode index

$$n_{eff_m} = k_m/k_o \quad .$$

For the waveguide described above, n_{eff} lies within the range

$$1.510 < n_{eff} < 1.523.$$

Each guided mode, upon incident on the grating, will be diffracted according to the equation

$$\sin\alpha + \sin\beta = \frac{\lambda}{dn_{eff}} \tag{11}$$

It is obvious that different waveguide modes will diffract into different directions even though they have the same incident angle. As far as the spectrometer operation is concerned this is equivalent to having an effective spread in optical wavelength.

A simple vector diagram illustrates the point more clearly. As shown in Figure 4-5, two wave vectors k_1 and k_2 are incident on a planar grating at an angle α with respect to the grating normal. Since k_1 and k_2 are of different magnitude and the change in wave vectors upon diffraction by the grating is the

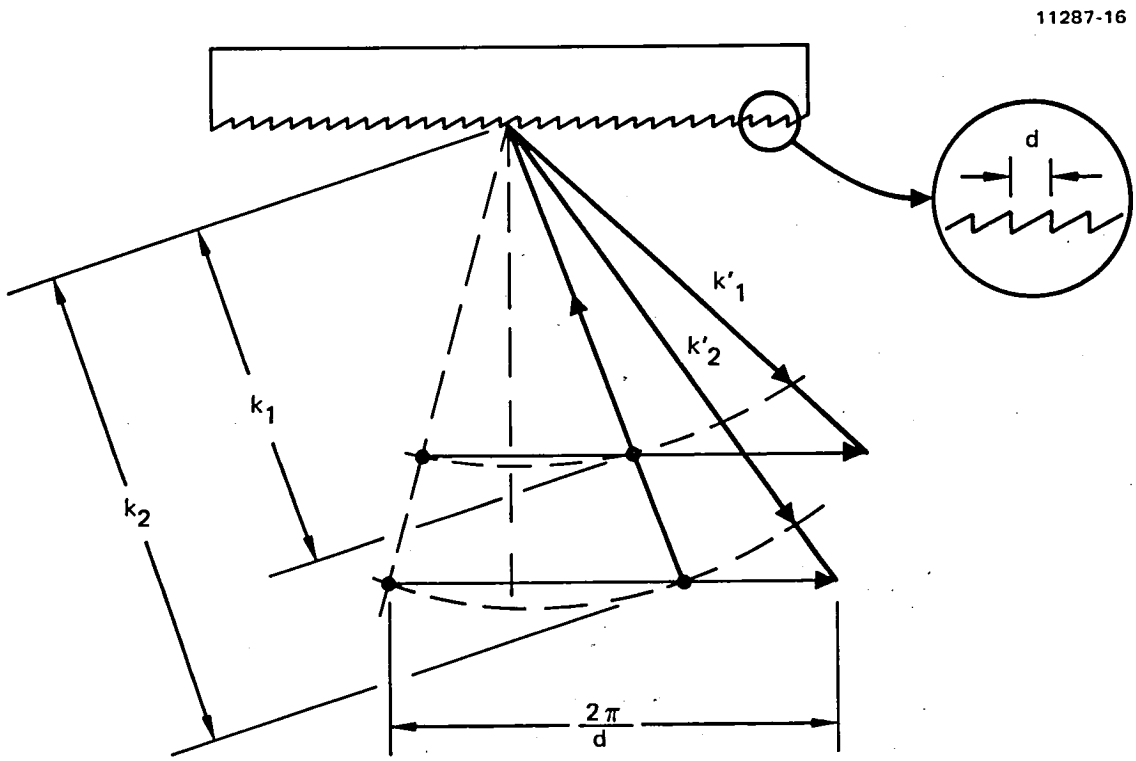

Figure 4-5. A vector diagram illustrating the diffraction of two waves with unequal wavevector.

same for both k_1 and k_2 ($\Delta k = \frac{2\pi}{d}$), the resultant vectors k_1' and k_2' will point in different directions as shown. We estimate the effective wavelength spread (worst case) for a waveguide layer with index of refraction n_2 surrounded by a medium of index n_1 using the formula

$$\Delta\lambda_{max} = \lambda \left(\frac{1}{n_1} - \frac{1}{n_2}\right). \tag{12}$$

With $\lambda = 0.83\ \mu m$ and $n_2 = 1.523$, we calculated $\Delta\lambda_{max}$ for a range of n_1 values. The results are listed in Table 4-2. The acceptable fiber N.A. is given by

$$(\text{Fiber N.A.})_{\text{glass to air}} = 1.523 \times (\text{Waveguide N.A.}).$$

Table 4-2. Calculated $\Delta\lambda_{max}$ For Different Waveguide Parameters ($n_2 = 1.523$)

n_1	1.520	1.517	1.514	1.510
$\Delta\lambda_{max}$, Å	11	22	32	47
Waveguide N.A. $(n_2^2 - n_1^2)^{1/2}$	0.10	0.14	0.16	0.20
Acceptable Fiber N.A.	0.15	0.21	0.24	0.30

It is clear from Table 4-2 that multimode waveguide dispersion can be a severe problem if high resolution demultiplexers are desired.

Our approach to solving the problem is to use a waveguide with a tapered thickness as shown in Figure 4-6. The thickness of the waveguide increases adiabatically from initial value of t_1 to a final value of t_2 over the entire device length R. The principle of this technique is as follows. Assume the thin waveguide can support N modes, their effective mode indices will lie throughout the range of $n_1 < n_{eff} < n_2$. If the waveguide thickness is allowed to increase adiabatically then the original modes of the thin waveguide will excite only the corresponding modes (same mode

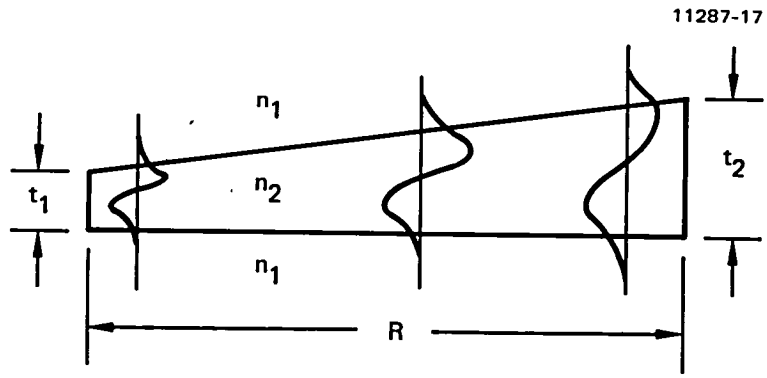

Figure 4-6. A waveguide structure in which the guiding layer thickness varies adiabatically from t_1 to t_2.

number) in the thicker waveguide. In other words, the adiabatic process does not allow mixing of guided modes to take place. At the thick waveguide end, the number of guided modes will be larger than N, but their mode indices still lie within the same limit, $n_1 < n_{eff} < n_2$. Therefore, as the modes of the thinner waveguide evolve into the modes of the thicker waveguide, the effective index of the mode changes continuously. Figure 4-7 shows an example of how the effective mode indices vary as the waveguide thickness is increased from 75 μm to 300 μm adiabatically. It is evident that the spread in n_{eff} is drastically reduced at the thick waveguide end. This result is summarized in Table 4-3.

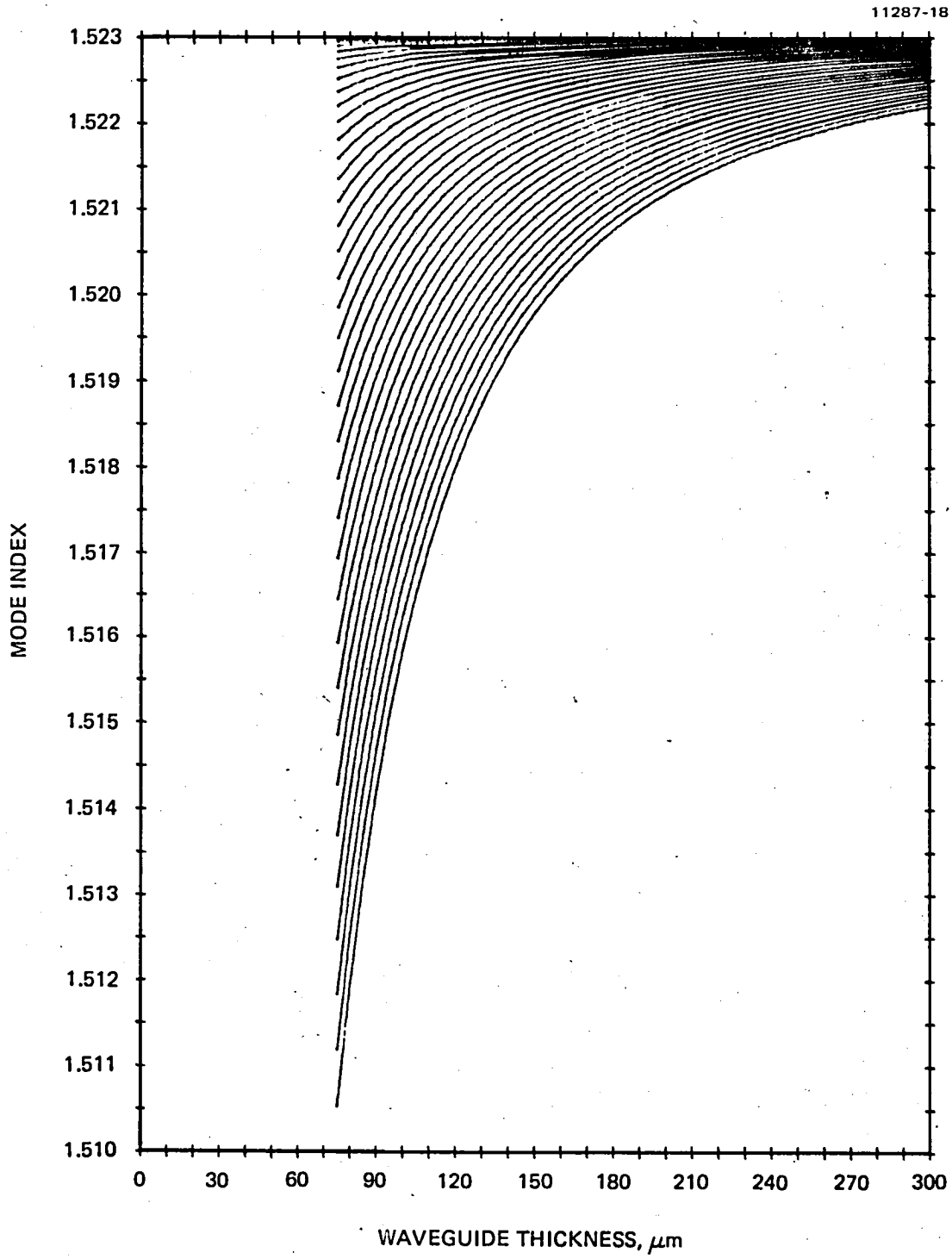

Figure 4-7. The effective mode index of each guided TE mode varies when the waveguide thickness is under adiabatic transition in its thickness.

Table 4-3. Calculated $\Delta\lambda_{max}$ as a Function of Waveguide Thickness (n_2 = 1.523, n_1 = 1.510)

Waveguide Thickness, μm	75	150	225	300
$(\Delta\lambda)$max Å	45	11.5	5.1	2.9

Thus, an effective wavelength spread of 45 Å in the 75 μm waveguide can be reduced to only 3 Å for a final waveguide thickness of 300 μm. The expense for this improvement is the increased waveguide loss (radiation loss) and the fabrication complexity. If the waveguide taper is not perfect, optical scattering can occur which results in the excitation of higher order modes as well as excessive radiation modes. This in turn will affect the device insertion loss and crosstalk isolation. A computer plot of a spectrometer output with a 55 μm wide uniform phase input radiation is shown in Figure 4-8. The parameters used are λ = 0.83 μm, R = 7.6 cm and a wavelength spread of 3 Å. Note that the aberration of the output spot, even in the presence of wavelength spread, is not significant. Futhermore, the signal level of the output spot outside of the 60 μm aberrated spot is quite low, which means good crosstalk isolation with adjacent channels.

In our device an inital waveguide thickness of 50 μm and a final thickness of 200 μm will be used over a device length of 7.6 cm.

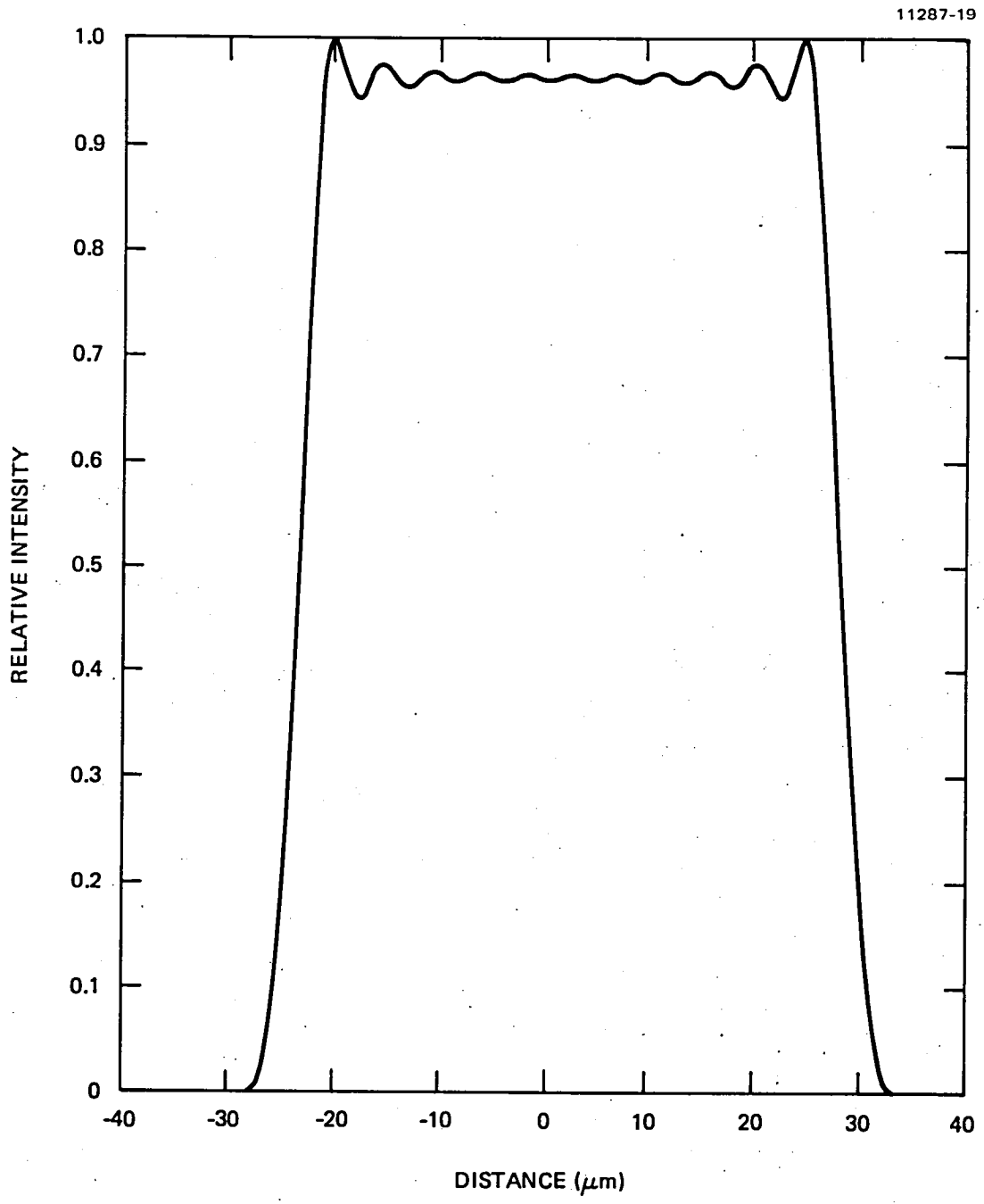

Figure 4-8. The calculated output spot profile of a modified Rowland spectrometer when illuminated by a 55 μm source of uniform intensity and phase.

SECTION 5

DEMULTIPLEXER FABRICATION AND TESTING

A. WAVEGUIDE FABRICATION AND CHARACTERIZATION

Since the tapered waveguide is a key feature in our demultiplexer design, we decided to carry out a preliminary experiment to fabricate and characterize such a structure. The purpose of this exercise is to determine the effectiveness of the approach in maintaining the lower order modes of the waveguide as well as to find out whether there will be any major technical difficulties in fabricating such a structure.

A piece of glass slide 2 inches long and 2 inches wide was cleaned thoroughly. After applying a thin layer of epoxy, a piece of cover glass was put on. Care was taken to drive the air bubbles out of the interface. The composite structure was then ground and polished to form a wedge as shown in Figure 5-1.

In order to launch light from the end face we have polished the two ends of the sample perpendicular to the waveguide-substrate interface. The waveguide thickness was then measured with a micrometer. It was found that at the thinner end the guide thickness was about 35.6 μm in the middle and tapered down to ~2 μm on one side and ~33 μm on the other side. The thick end of the guide, however, was more uniform and measured to be ~254 μm. Thus the wedge angle of the guiding layer in this case turned out to be ~0.25°.

The waveguide sample was then tested in the arrangement illustrated in Figure 5-2. A He-Ne laser was coupled into a graded index fiber with a 55 μm core diameter and the fiber was butt coupled to the thin edge of the sample. The output of the tapered waveguide was displayed on a white screen ~5 cm away from the thick edge of the sample. On the screen we observed an illuminated band about 2 mm wide which corresponded to an output divergence angle of ~2°. For comparison we set up a flat planar waveguide that consisted of a thin cover glass sandwiched between two

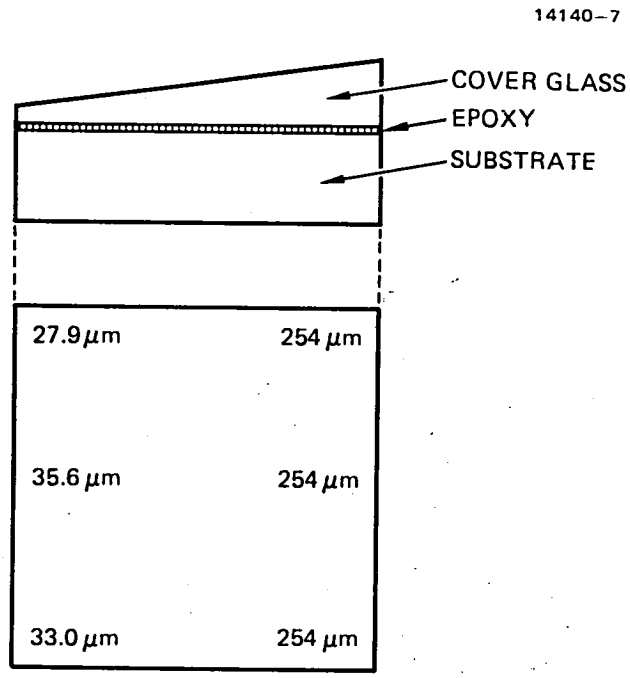

Figure 5-1. The tapered waveguide used in the experiment. The numbers shown indicate the actual waveguide thickness.

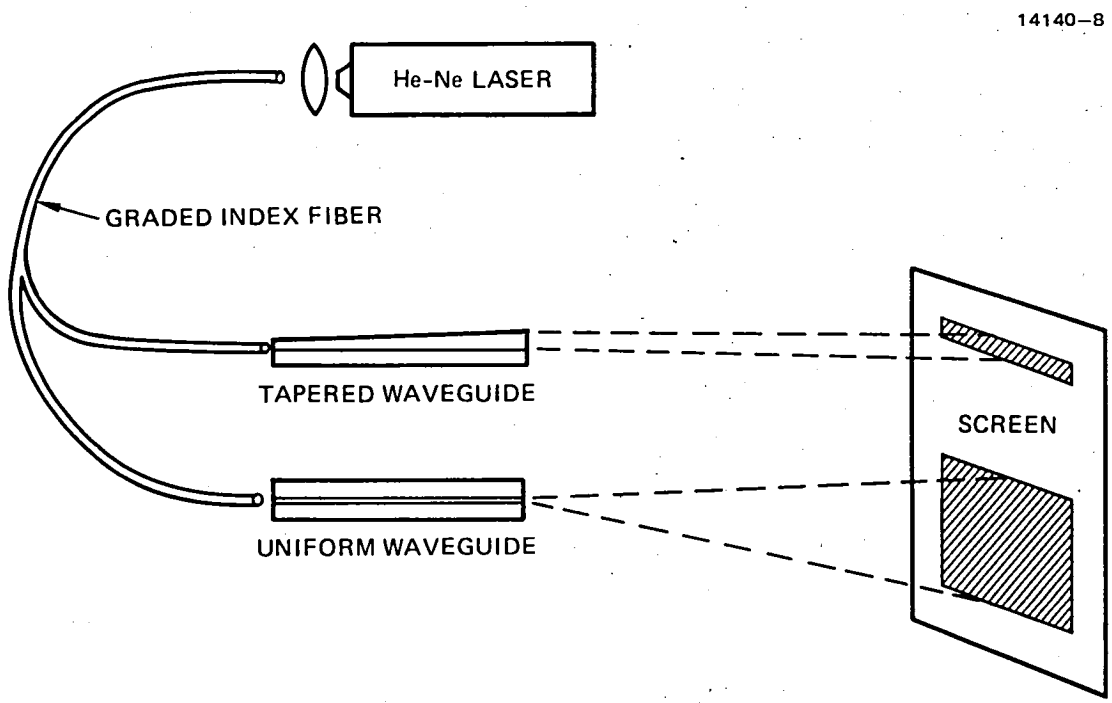

Figure 5-2. Experimental setup for observing the collimating effect of tapered waveguide.

glass slides. The thickness of this guide was 67 μm. When excited in a similar manner, the output pattern of this waveguide measured 17 mm wide and corresponded to a beam divergence angle of 19.3°. It is evident that by tapering the waveguide thickness we achieved the desired collimating effect. Although the tapered waveguide exhibited a slight increase of surface scattering, we believe that by the addition of a superstrate, this problem will be alleviated.

One of the potential problems in the fabrication process is the uniformity of the waveguide layer after wedge polishing. This stems from the fact that the epoxy layer between the cover glass and the substrate is nonuniform. We anticipate that a more evenly applied pressure during the epoxy drying process will improve the situation. Small and gentle variations in waveguide thickness should not introduce excessive radiation loss.

After the initial confirmation of tapered waveguide function, we proceeded to procure the glass slides. These included 20 pieces of 4 in. x 4 in. x 0.09 in. master grade electromask blank substrate, 10 pieces of 4 in. x 4 in. x 0.02 in. electromask blank substrate from Telic Corporation and 40 pieces of 2 in. x 4 in. cover glass slides (#3 thickness) from J. Melvin Freed Company. The thicker blank substrates will be used for the top and bottom plates of the sandwiched waveguide structure and the thin cover glass slides will be the actual waveguiding region.

Since the waveguide layer needs to be lapped and polished to form a wedge in our design, it is important that the epoxy layer between the thin glass wafer and the thick substrate be reasonably flat. To assure this, we carefully measured the thickness of both glass plates at various points. The thickness variation was found to be less than ±2.5 μm for most parts of the wafer.

After thorough cleaning, the epoxy was applied. Air bubbles were initially driven out with finger pressing. The composite structure was then put in between two anodized plates and pressed with lead brick (9 1/2 kg) for 2 to 3 hours. The thickness of the laminated sample was then measured again. Taking the difference of this reading and the combined readings taken previously, we estimated the epoxy film thickness.

Several methods were tried to increase the film thickness uniformity with varying degrees of success. Initially, the epoxy film can vary from 3 μm on one side to 20 μm on the other side. The improved device was able to keep the variation to below 10 μm. Our starting material has a dimension of 4 in. x 2 in. which is bigger than the final device size of 3 in. x 1.5 in. Therefore, the edges of our sandwiched structure will be trimmed off during fabrication. This should help to improve the waveguide thickness uniformity.

After grinding and polishing we were able to determine the typical thickness of the wedged-waveguides to be $\sim$60μm on one end and $\sim$245 μm on the other end over a length of 8.5 cm, yielding a slope angle of $\sim$0.12°. We proceeded to put the superstrate (0.009 in. thick glass plate) on these tapered waveguide samples to complete the structure. The waveguides were then sent to Rainbow Optics for grinding and polishing to form the curved waveguide ends. After receiving the finished devices, various geometrical parameters of the waveguides were measured and the optical quality of the two curved edges were examined carefully. The results are given in Table 5-1 with the waveguides labeled from W-1 to W-10. The meanings of the symbols are indicated in Figure 5-3.

From the chart we concluded that the waveguide quality was not as good as we would like to have, especially the front facets and the waveguide length. We hope that using epoxy between the fibers and the waveguide front edge in the final device might alleviate the potential scattering problem.

Table 5-1. Waveguide Dimensions and Edge Quality

(All Numbers Are In Inches)							Edge Quality	
Waveguide Number	L	W	L_1	L_2	t_1	t_2	Front	Back
W-1 (S)	2.998	1.505	2.706	2.702	0.190	0.196	Upper Half:Chips Lower Half:Ok	Ok
W-2 (S)	2.998	1.504	2.706	2.706	0.190	0.1955	Chips	Ok
W-3 (S)	2.999	1.504	2.707	2.707	0.1905	0.196	Rough Edges	Ok
W-4 (C)	3.002	1.504	2.703	2.703	0.188	0.1925	Chips	Upper Half:Chips Lower Half:Ok
W-5 (C)	3.001	1.504	2.703	2.703	0.1905	0.1955	Ok	Upper Half:Ok Lower Half:Chips
W-6 (S)	3.000	1.504	2.700	2.708	1.189	0.1945	Upper Half:Chips Lower Half:Ok	Ok
W-7 (C)	2.999	1.504	2.697	2.710	0.1885	0.1945	Small Chips	Small Chips
W-8 (S)	2.999	1.504	2.705	2.705	0.1885	0.1945	Small Chips	Ok
W-9 (C)	2.998	1.504	2.703	2.703	0.1895	0.1945	Edge Chipping	Ok
W-10 (S)	2.995	1.504	2.704	2.698	0.1865	0.1925	Chips	Ok

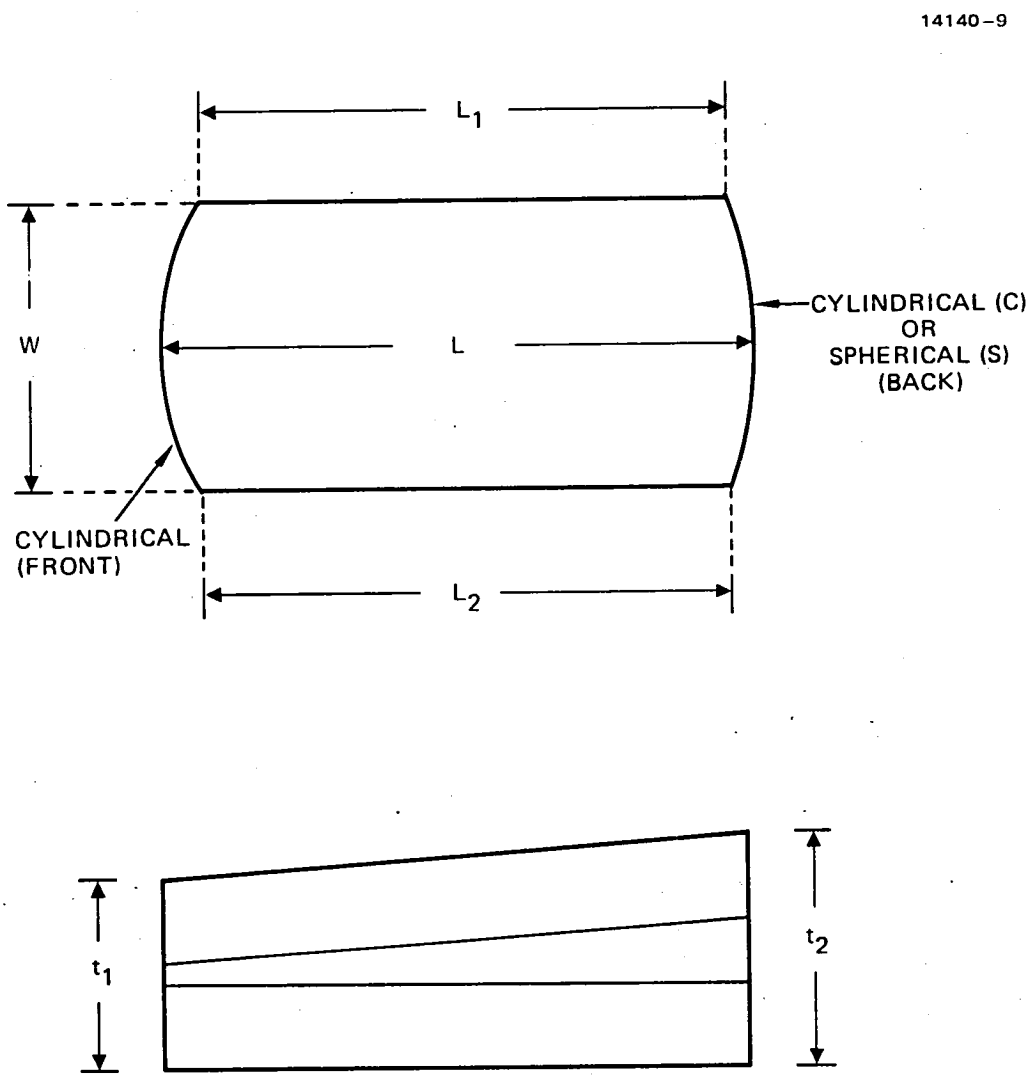

Figure 5-3. Demultiplexer waveguide geometry.

The demultiplexer waveguides were characterized by excitation with a 55-μm core multimode fiber, after which the reflected spot size was recorded. Under ideal conditions, the Rowland planar structure acts as a one-to-one imaging system. Therefore, we expect the measured spot size to be comparable to that of the input excitation. As pointed out previously, most of the samples have lengths shorter than the desired 7.62 cm. Therefore, we expect the output spot size to be larger than the excitation source size. For measurement and comparison purposes, we fixed the input fiber to be in contact with the waveguide edge. The output spot was scanned with a 4.5-μm core single-mode fiber. The location of the single-mode fiber tip can be adjusted from a point just touching the waveguide up to a distance of 2 mm away from the guide edge.

All samples were examined carefully. The output fiber was moved in and out to search for the apparent focused spot. The measured results are summarized in Table 5-2. We conclude from these results that the waveguide quality was not as good as we anticipated. The blemishes in waveguide edge polishing and the dimensional errors of the guides definitely contributed to the cause of large output spot size. The waveguides with cylindrical end faces are especially poor.

B. GRATING FABRICATION AND TESTING

Based on the calculations given in Section 4, we designed a spherically concave grating with the following specification: (1) a radius of curvature of 7.62 cm; (2) a grating constant of 1.6 μm (~630 lines/mm); (3) an input fiber incident angle of 6° at λ = 0.83 μm; and a corresponding diffraction angle of 11.94°. Using these numbers together with the physical dimensions of the waveguide (3 in. x 1.5 in.), we obtained a linear dispersion of our planar Rowland spectrometer to be ~3.00 μm/Å, suitable for high resolution wavelength division multiplexing use.

Table 5-2. Summary of Waveguide Evaluation

Sample No.	Location of the Minimum Spot (mm From the Waveguide Edge)	Minimum Spot Size (μm)
W - 1	0.76	70.6
W - 2	0.50	77.1
W - 3	0.37	69.2
W - 6	0.00	137.2
W - 8	0.00	140.0
W - 10 (Cylindrical - spherical ends)	0.90	116.4
W - 4	0.17	257.0
W - 5	0.045	186.8
W - 7	0.08	206.0
W - 9 (Cylindrical ends)	0.00	165.4

As indicated in Figure 5-4, the grating blaze angle required for high efficiency performance is calculated as

$$\theta - \alpha = \beta - \theta$$

or

$$\theta = (\alpha + \beta)/2 \quad ,$$

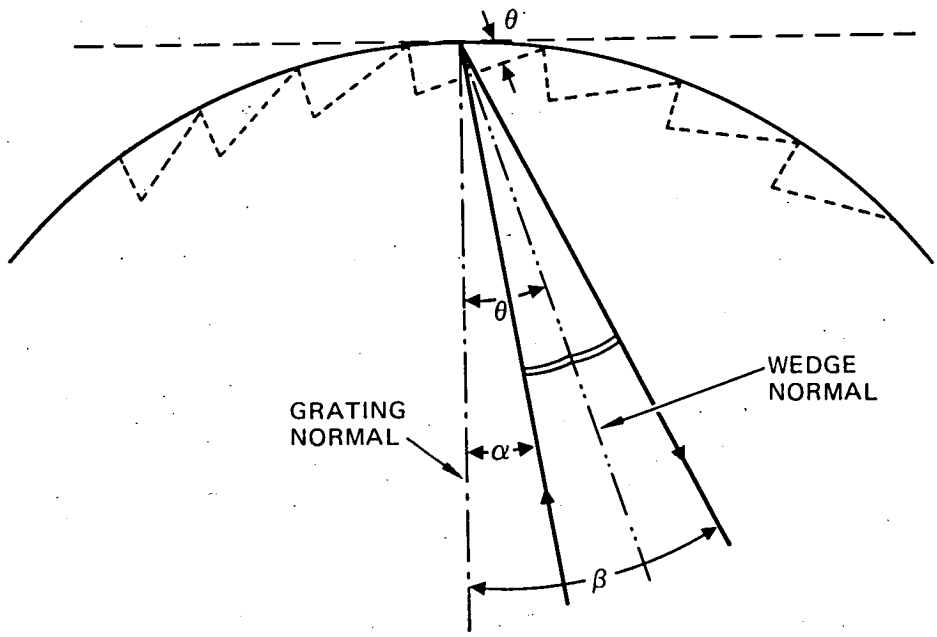

Figure 5-4. Relations of α, β, and θ.

where θ is the desired blaze angle, α is the incident angle and β is the diffracted angle. For our design, $\alpha = 6°$ and $\beta = 11.94°$; therefore, $\theta = 8.97°$. The physical dimensions of the grating block is 1 cm x 1 cm x 4 cm and the ruled area is 0.5 cm x 3 cm, as shown in Figure 5-5.

Diffraction Products, Inc., of Woodstock, Illinois, was selected to fabricate these special gratings. After some initial delays, we received the first replicated concave grating. A careful examination of this grating was carried out by measuring its diffraction efficiency and taking both optical and scanning-electron-microscope photographs.

The grating was ruled in four sections, as shown in Figure 5-6. Sections 1 through 3 are 7.5 mm long each, while Section 4 is only 5 mm long. There are several tiny voids in the grating and there is a scratch ~0.4 mm wide and 6 mm long in Section 3. Between Sections 1 and 2, there is a gap of ~0.1 mm.

14140–11

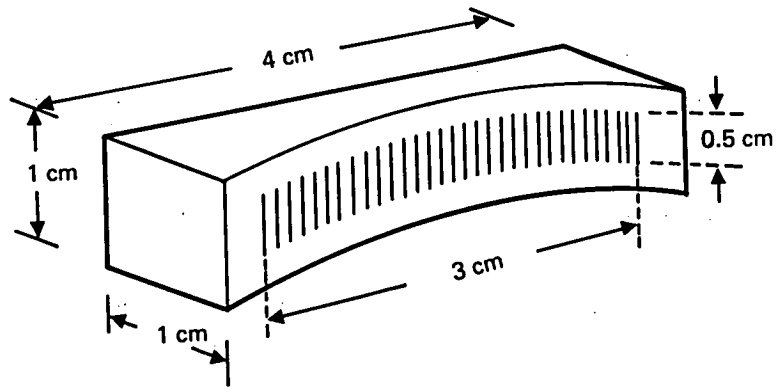

Figure 5-5. Dimensions of the concave grating.

14140–12

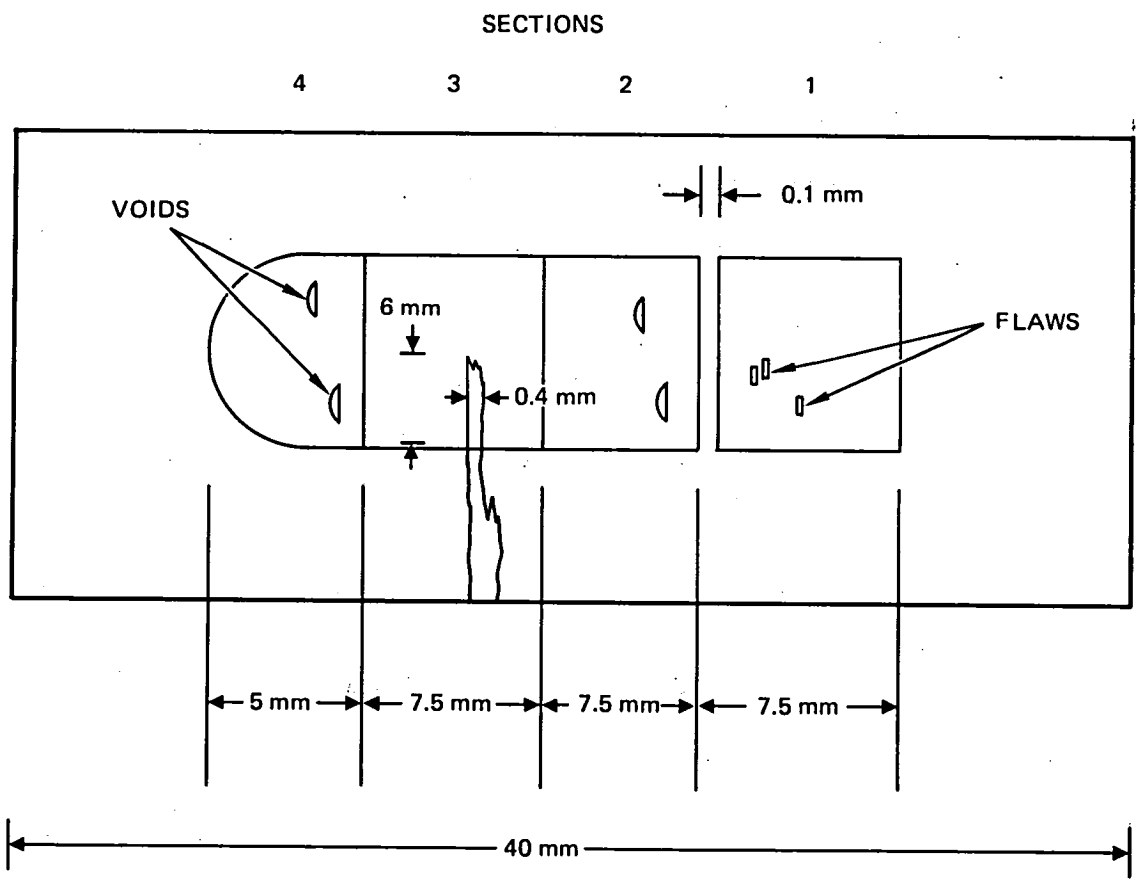

Figure 5-6. Grating geometry and locations of various defects.

The grating diffraction efficiency was measured with a collimated GaAs laser, illuminating the 4 sections individually. The overall diffraction efficiencies of the grating sections are 72.9%, 79%, 79.7% and 75.6%, respectively. However, the majority of the diffracted power is in the zeroth order. Diffraction efficiency for the desired -1 order is only around 3%.

Several SEM pictures were taken in an attempt to visualize the groove shape and to correlate this information with the measured diffraction efficiency results. Upon close examination we noticed that the grooves had a flat top. Therefore, the groove profile resembles a trapezoid rather than a triangle. This may result in a lower diffraction efficiency in the desired order than anticipated.

Diffraction Products, Inc. agreed to make a second run and apply slightly larger pressure on the diamond tip to ensure a deeper groove and proper profile.

After much delay, we finally received two of the replicated concave gratings. According to the manufacturer, the grooves are deeper than the previous ones. However, the blaze angle is correct only near the center of each ruled section as before.

Diffraction efficiency of the gratings were measured using a collimated 1.3 μm semiconductor laser (HLP 5400) beam in air. For our application, the -1 diffraction order is the most improrrtant one. The diffraction efficient varies among the four sections of the concave grating with an average efficiency of ~9% into the -1 order. This will yield a 10.5-dB demultiplexer throughput loss due to the grating alone. It appears that ruled diffraction gratings on a small radius of curvature (7.5 cm in this case) require additional development work.

There are two other possible approaches for obtaining high efficiency gratings. The first uses preferential etching of a thin silicon wafer with appropriate crystal orientation to achieve the desired blaze angle. A second approach is to use a planar (replicated) blazed grating with a thin, flexible substrate (such as cover glass).

Both approaches require the bending of the grating to conform to the waveguide end curvature. For this purpose, the grating substrate should be thin (<100 μm) to avoid breakage.

The glass substrate is the preferred approach because of its simplicity. The silicon etched grating is unique, but the technical difficulty is far too great and the improvement over the glass substrate approach may not be significant.

We have also evaluated some flexible gratings with epoxy backing. The flexibility and durability of these gratings are suitable for bending to a small radius of curvature. However, the grating surface tends to be distorted from handling. We therefore concluded that a thin glass substrate that is both rigid and flexible should be used. Thus a first batch of replica gratings on glass substrate were ordered and received. The substrate for the grating is a cover glass with a thickness ~125 μm; the diffraction efficiency of the -1 order was measured to be ~65% (-1.87 dB).

The grating was carefully scribed and broken into strips of 4 cm x 0.5 cm. This is a convenient size for handling and attachment to the waveguide edge. Experiments were carried out to determine the optimal method for mounting the grating to the waveguide so that a "clean" output spot could be obtained. The most common problem in mounting the grating is the error in bending curvature. Although efforts were made to conform the grating to the waveguide end curvature, it is still difficult to consistently achieve good output.

It appears that a substantial amount of pressure is required to ensure optical contact between the grating and the waveguide. This often resulted in grating breakage. We believe that using an even thinner glass substrate (~80 μm) should alleviate this problem. Several of these new gratings were received and evaluated. The total diffraction efficiency was measured to be ~74% (-1.31 dB), while the diffraction efficiency for the desired order (m = -1) is ~63% (-2 dB).

The supplier indicated that because of the thin substrate, the replication process had to be done differently: the replica gratings were peeled off the submaster slowly as opposed to the separation process used for conventional thick substrate gratings, causing, it was suggested, distortions and damages to the grating surface. This, in turn, would yield a low overall grating efficiency.

We proceeded to experiment with various ways of attaching gratings to the planar waveguides permanently. The gratings are initially attached to the waveguides with adhesive tapes. The waveguide is then secured inside an aluminum fixture, as shown in Figure 5-7. The space between the grating and the end of the fixture will be occupied by pressure pads.

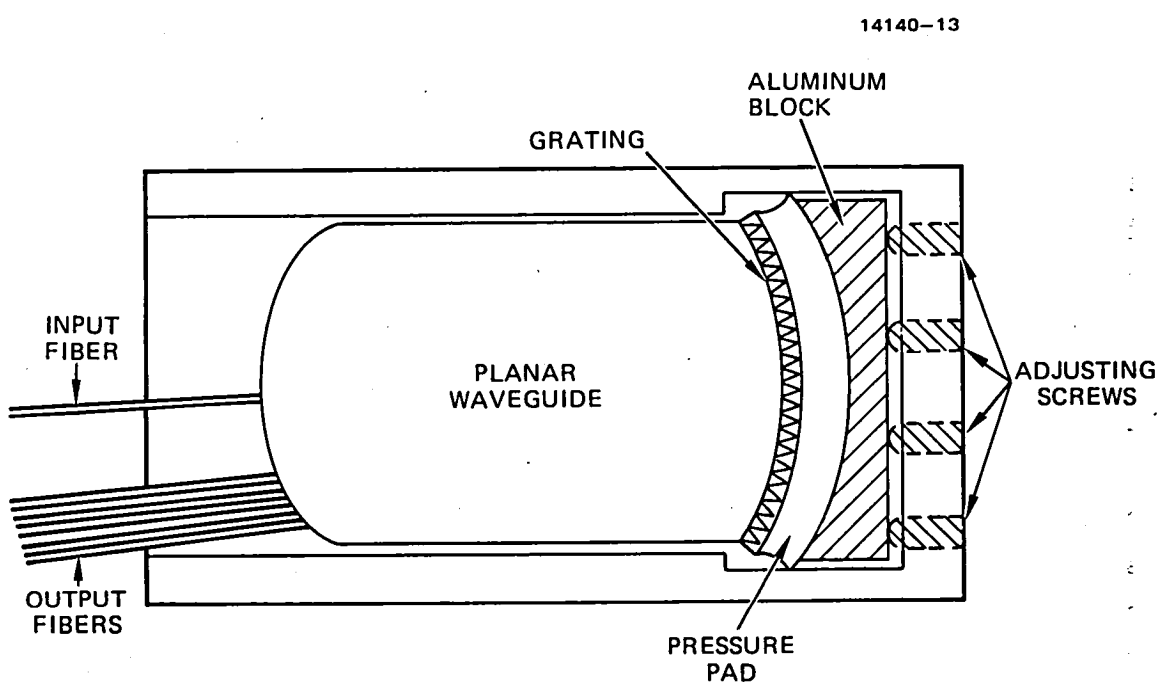

Figure 5-7. Demultiplexer Housing

We first tried to fill up the space with Eccofoam FPH, hoping that the pressure developed during the foaming process would be sufficient to press the grating firmly against the guide. However, it was found that the pressure developed was insufficient.

After a few more attempts of using different foaming agents we settled on a process that yielded fairly consistent results. Four screws were installed in each waveguide fixture and used to apply pressure to the grating through a plastic pressure pad (Sylgard 182). Multiple screws allow some tunability; minimizing the output spot size is a criterion for optimization.

The completed waveguide-grating structures were characterized by excitation with a 50 μm-core fiber carrying 0.83 μm radiation. The output intensity was then plotted from a 100 μm-core fiber as it was scanned across the output port of the device. All four demultiplexers showed similar traces, indicating good uniformity among the devices (see Figures 5-8 through 5-11). Note that the traces are not symmetric. We believe that the long tail is due to intrinsic aberrations of the Rowland structure. We have also obtained some quantitative measures of the module insertion loss, ranging from 7.2 to 9 dB, as well as crosstalk isolation of about 20.5 dB for output fibers 300 μm apart. Both the insertion loss and crosstalk performance of the demultiplexers should improve when index matching epoxy is used between the fibers and the planar waveguide.

C. DEMULTIPLEXER PACKAGING AND CHARACTERIZATION

The spectral resolving power of the demultiplexer is further characterized using the arrangement shown in Figure 5-12. A tungsten halogen lamp white light source is focused into the entrance slit of a 1/4-spectrometer. The output of the spectrometer is focused into the 55-μm core input fiber of the demultiplexer.

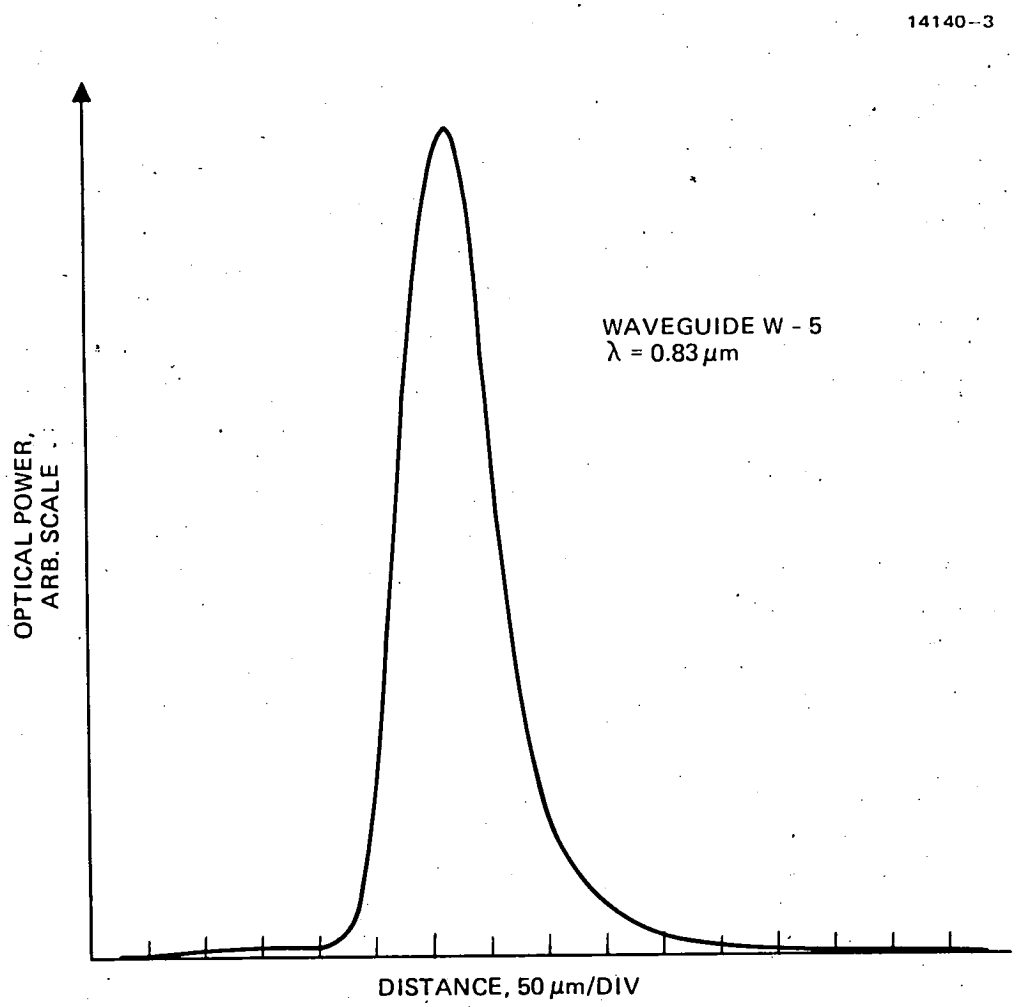

Figure 5-8. Optical power versus output fiber location trace for W - 5.

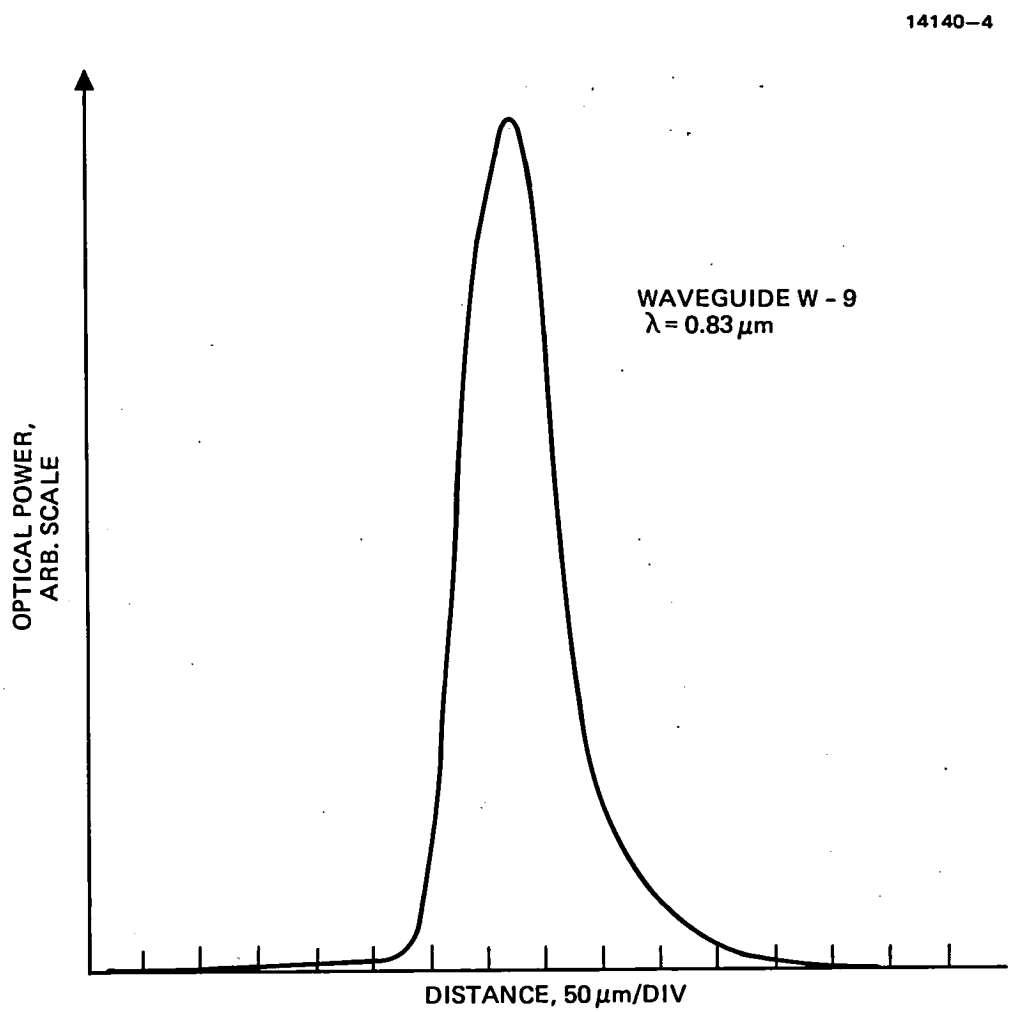

Figure 5-9. Optical power versus output fiber location trace for W - 9.

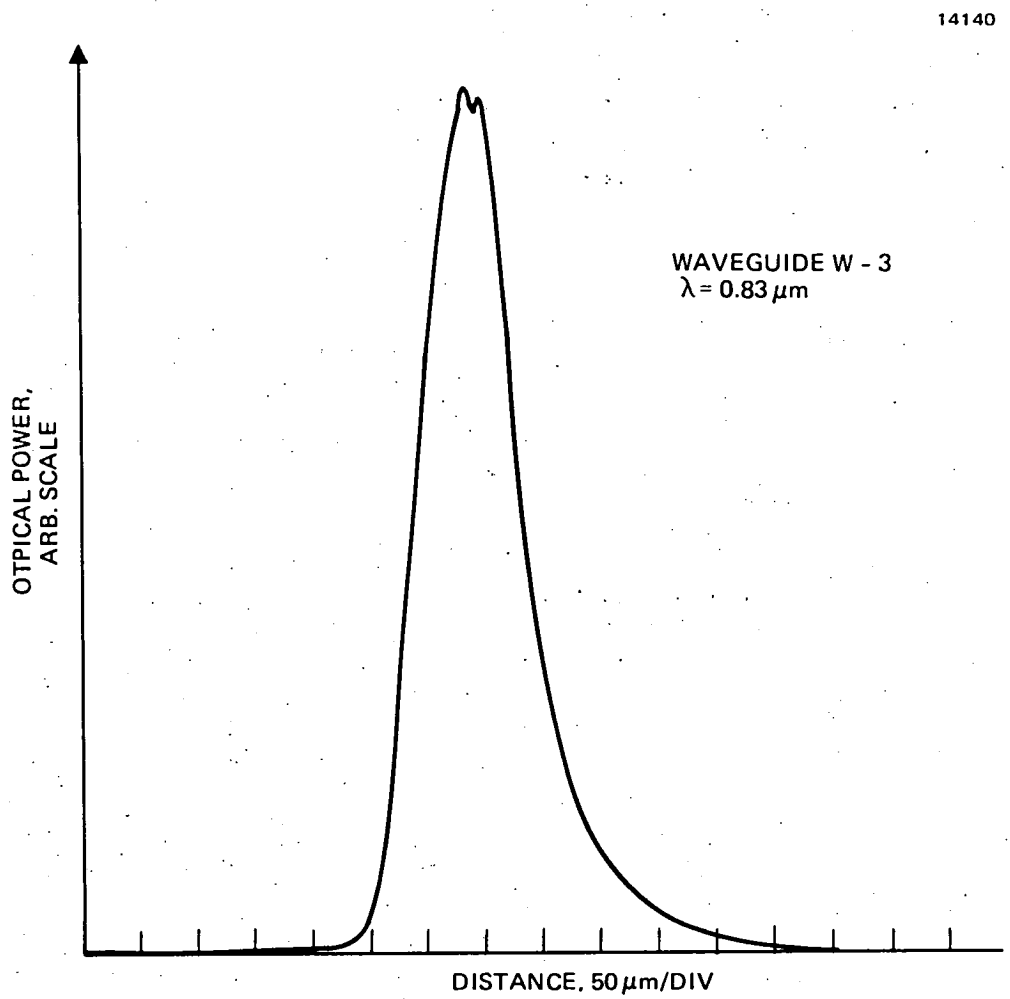

Figure 5-10. Optical power versus output fiber location trace for W - 3.

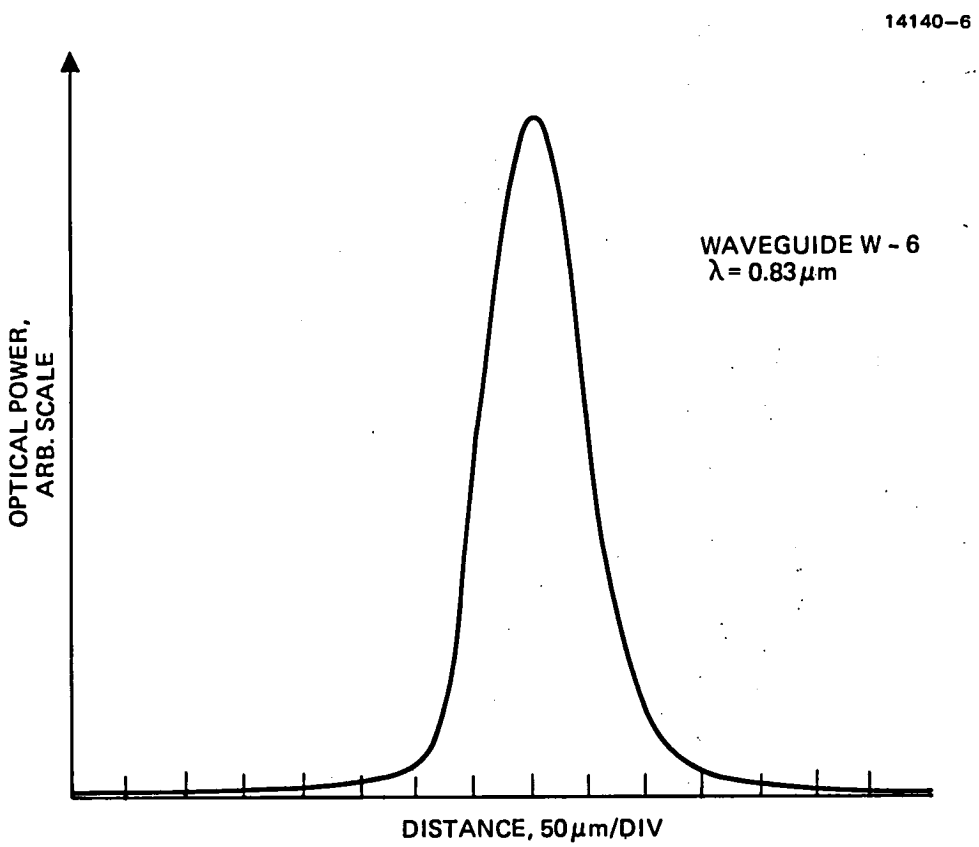

Figure 5-11. Optical power versus output fiber location trace for W - 6.

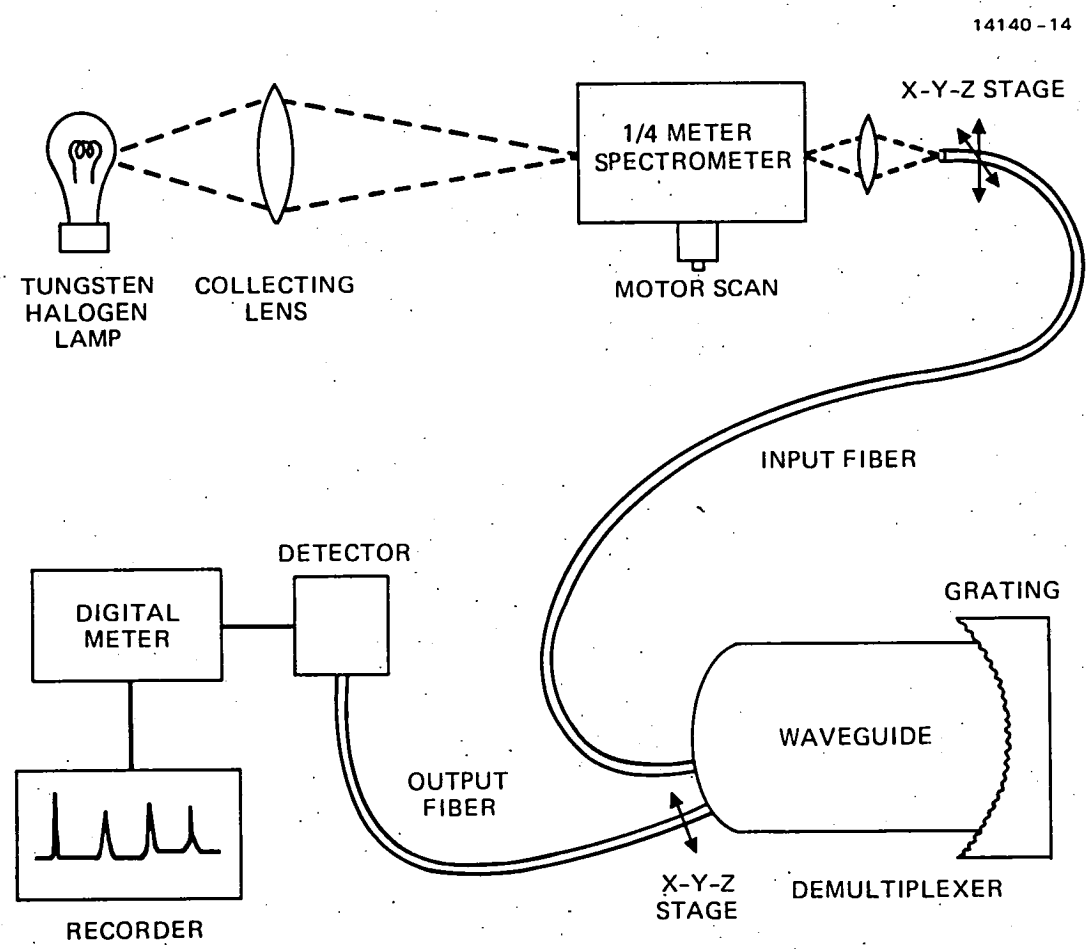

Figure 5-12. Experimental arrangement using white light source.

The slit width of the spectrometer is set to be 250 μm so that sufficient optical power is collected by the fiber. The spectrometer setting can be adjusted so that radiation wavelengths of 8100 Å, 8200 Å, 8300 Å and 8400 Å are sequentially selected. At the output of the demultiplexer, the 100-μm core output fiber is scanned across the waveguide edge and the traces are recorded for each spectrometer wavelength setting. The results are shown in Figure 5-13. As we can see, the four wavelengths with 100-Å separations are clearly resolved. The spatial separation of the peak locations are ~300 μm. We believe that the apparent uneven separations are due to errors in spectrometer wavelength settings caused by backlash.

The results obtained in this experiment will be used to design the output fiber configurations so that they are properly spaced and with optimal coupling.

To complete the demultiplexer assembly we have to attach both the input and output fibers to the waveguide. The input fiber is relatively easy to handle and design because only one fiber is involved. The output end is more complicated because each output fiber must be coupled to a specified wavelength.

Two factors are important here: one is the fiber separation; the other is the mechanical stability. Due to an error in waveguide edge polishing, the total guide length is shorter than the desired value. Consequently, the output spots do not have minimum waist on the waveguide edge. Instead, the optimum position of the output fiber is ~310 μm away from the waveguide. Therefore, the output fibers cannot be expoxied directly to the guide and must be supported somewhere else. In this case, it is important to determine how much cantilever is tolerable beyond the point of support, which should be as short as possible without interfering with the positioning of the fiber ends.

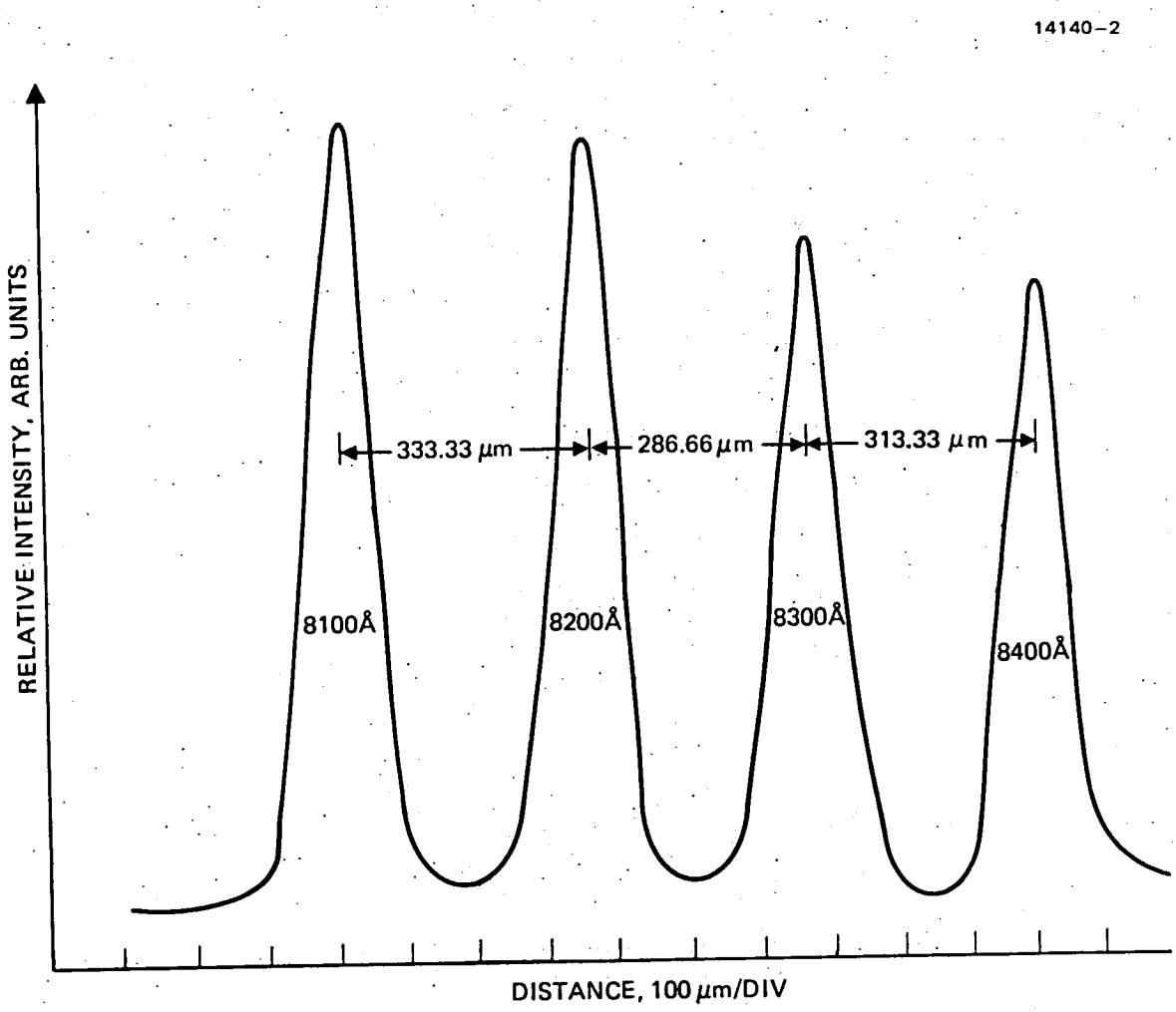

Figure 5-13. Spatial distribution of the 4 desired wavelength.

Since it is impractical to try to align each of the four output fibers individually, we decided to use a linear fiber array at the output port. One way of forming a linear fiber array of proper spacing is to use a precision V-grooved silicon plate for alignment. A simpler but less precise method is to arrange fibers in a linear array with minimum gap between fibers. The array will contain four actual output fibers plus some "spacer fibers". In principle, one can use fibers of different outer diameters to obtain any desired output fiber spacings. However, our experimental results indicated that if the difference between the fiber diameters is too large, it would be difficult to keep the small diameter fibers in their proper positions. Best results were obtained by using same-size fibers in the array.

We also applied a unique technique (developed at HRL for a different application) to form a ruggedized fiber array. After arranging the fibers into a tight linear array, we encapsulated the entire array in copper through an electro-forming process. Each array contains four output fibers (100 μm core diameter, 140 μm outer diameter) separated from each other by $\sim$280 μm. Figure 5-14 shows part of an array, indicating the position of fibers relative to the edge of copper. Figure 5-15 shows the fiber array with four output fibers with their cores illuminated. Note that the fiber ends are completely embedded in copper. It is relatively easy to polish fiber ends.

Because of the rigidity of the array it can be mounted directly on the adjustable mount inside the demultiplexer package. To align such an array we typically excite the input fiber with at least two wavelengths (λ_1 and λ_2) simultaneously: λ_1 corresponds to fiber No.1 in the array; λ_2 corresponds to fiber No. 4 in the array. Thus, if the outputs of fiber No. 1 and No. 4 are maximized simultaneously, then fiber No. 2 and No. 3 will be in perfect alignment as well. Once an optimal condition is reached, all the fibers are epoxied to the case of the module. A sequence of photographs illustrating the demultiplexer packaging is shown in Figure 5-16.

14140–15

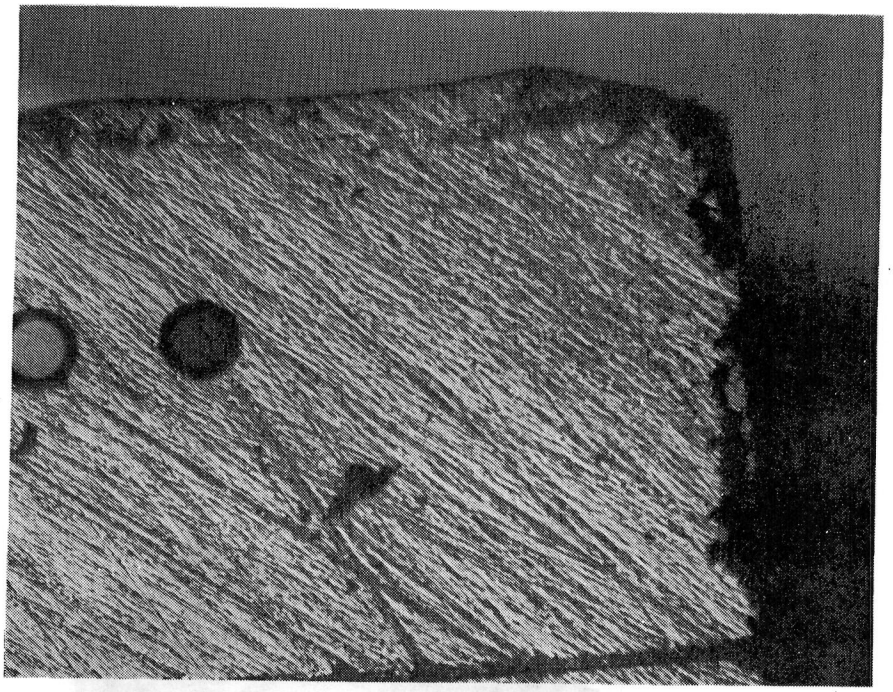

Figure 5-14. Copper encapsulated fibers showing the edge of copper.

14140–16

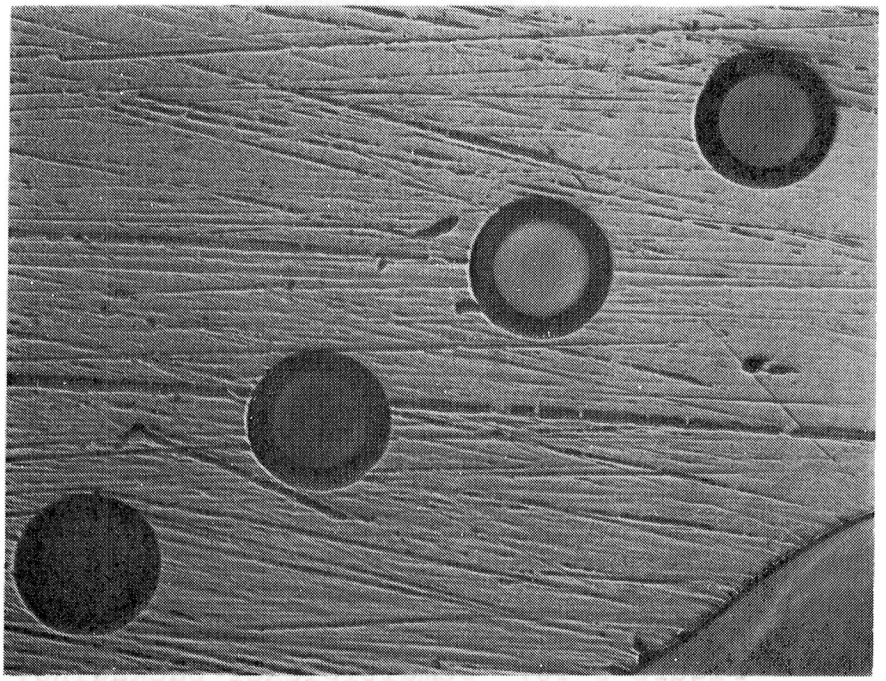

Figure 5-15. Polished end of fiber array.

14140—18

(a)

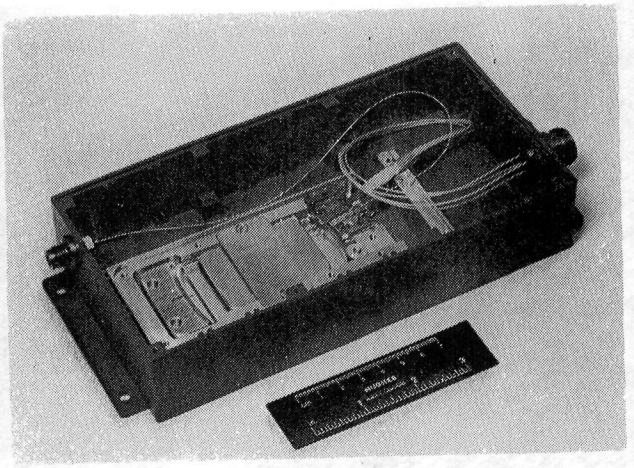

(b)

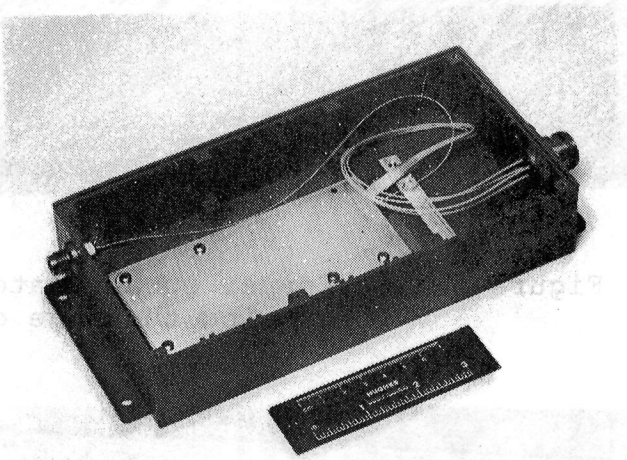

(c)

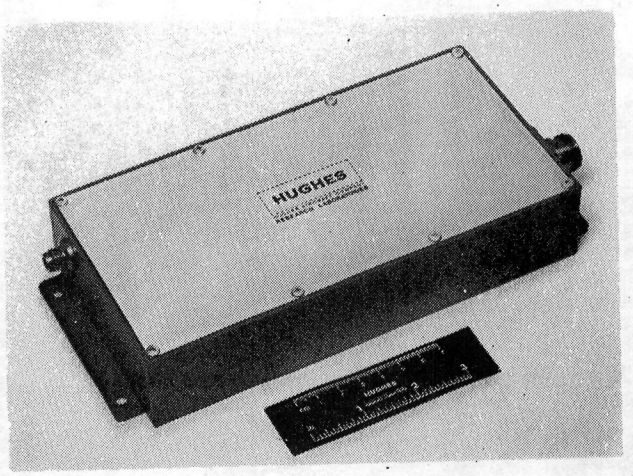

Figure 5-16. Demultiplexer packaging.

Once the demultiplexers are packaged, the passband of each channel is checked again using a white light source and a spectrometer. The peak wavelengths of the demultiplexer outputs are indicated in Figure 5-17. The wavelength, of the four channels were set at 8050 Å, 8150 Å, 8250 Å, and 8350 Å. However, the figure clearly shows a rather wide range of scattering in peak wavelengths. The sources of error are deviations in fiber array positioning and irregular fiber spacings in the array. The peak wavelength deviations will contribute to the overall insertion loss and crosstalk isolation degradations.

The demultiplexers are also tested using semiconductor lasers with peak wavelengths tuned to ~8050 Å, 8250 Å, and 8350 Å. These wavelengths were used because of the availability of the diodes. The cable is connected to the input ports of the demultiplexers. The outputs from the demultiplexers are then measured and computed to indicate insertion loss and crosstalk levels (see Table 5-3).

The poor insertion loss stems mainly from excessive aberrations in the device as seen in the traces shown in Figures 5-8 through 5-11. The measured numbers are further worsened by the total emission spectral width of the lasers. This is evident when a spectrometer is used to filter the 8050 Å and 8350 Å laser outputs before launching into the demultiplexers. Crosstalk reduction of between 7 and 10 dB are obtained (the new crosstalk numbers are given in parentheses).

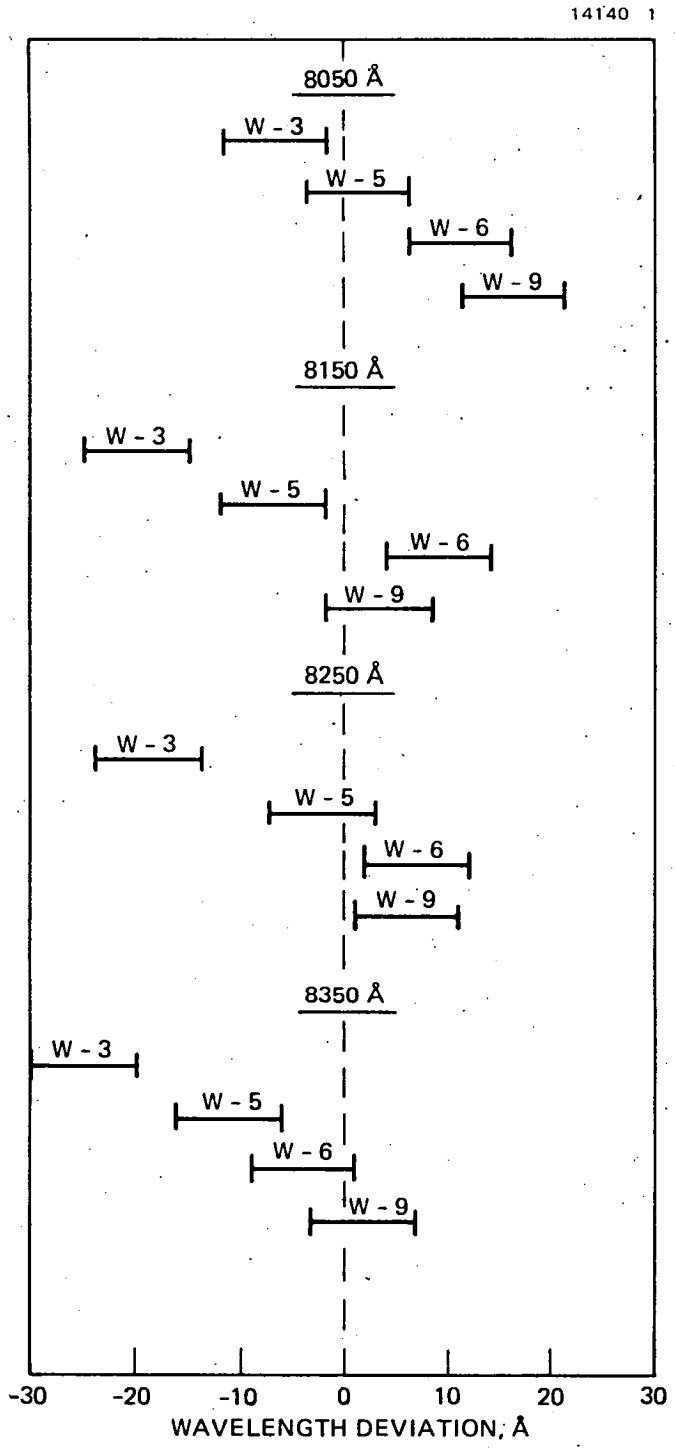

Figure 5-17. Wavelength deviations in packaged demultiplexers.

Table 5-3. Demultiplexer Crosstalk (CT) and Insertion Loss (IL) Characteristics

W 3

Input \ Output	Ch. 1 (8050 Å)	Ch. 2 (8150 Å)	Ch. 3 (8250 Å)	Ch. 4 (8350 Å)
8050 Å	IL -16.7 dB	CT -5.4 dB (-15.4 dB)	CT -10.4 dB	CT -15.2 dB
8250 Å	CT -20.7 dB	CT -16.5 dB	IL -20.8 dB	CT -7.0 dB (-10.2 dB)
8350 Å			CT (-27.4 dB)	IL -20.6 dB

W 5

Input \ Output	Ch. 1 (8050 Å)	Ch. 2 (8150 Å)	Ch .3 (8250 Å)	Ch .4 (8350 Å)
8050 Å	IL -18.4 dB	CT -6.7 dB (-13.0 dB)	CT -9.3 dB	CT -13.6 dB
8250 Å	CT -23.1 dB	CT -21.1 dB	IL -20.0 dB	CT -8.2 dB (-10.5 dB)
8350 Å			CT (-20.0 dB)	IL -16.2 dB

Table 5-3. Demultiplexer Crosstalk (CT) and Insertion Loss (IL) Characteristics (Continued)

W 6

Input \ Output	Ch. 1 (8050 Å)	Ch. 2 (8150 Å)	Ch. 3 (8250 Å)	Ch. 4 (8350 Å)
8050 Å	IL -17.3 dB	CT -7.0 dB (-15.0 dB)	CT -10.1 dB	CT -13.5 dB
8250 Å	CT -18.8 dB	CT -17.5 dB	IL -16.2 dB	CT -11.5 dB (-12.3 dB)
8350 Å			CT (-18.9 dB)	IL -12.4 dB

W 9

Input \ Output	Ch. 1 (8050 Å)	Ch. 2 (8150 Å)	Ch. 3 (8250 Å)	Ch. 4 (8350 Å)
8050 Å	IL -18.0 dB	CT -5.6 dB (-15.6 dB)	CT -10.7 dB	CT -15.4 dB
8250 Å	CT -24.1 dB	CT -19.6 dB	IL -19.4 dB	CT -10.5 dB (-13.4 dB)
8350 Å			CT (-27.2 dB)	IL -15.3 dB

SECTION 6

FABRICATION OF 4 X 4 STAR COUPLERS

A 4 x 4 fiber optic start coupler can be used as a wavelength-insensitive multiplexer for four input wavelengths. Since all four ports are utilized, it can be quite efficient as well. In the past the couplers were fabricated using a simple fixture that accepts a group of 4 fibers; with one end of the fibers clamped down, the fibers were twisted slightly and then flame-fused together under axial tension. The twisting is to ensure that the fibers stay together when heated. One of the major difficulties has been the lack of uniformity in output power distribution. The launching fiber invariably retains the largest portion of the input optical power. A second problem is the movement of fibers during heating since it always introduces a kink in the tapered region of the coupler, which results in a higher insertion loss.

We have since modified our set-up by adding a rotatable quadrant separator to maintain a fixed spatial relationship among the fibers. After the fibers are in place the separator is rotated to introduce a controlled amount of twist. The fibers are then fixed in place with fast cure epoxy at both ends. Repeated experiments showed that the coupling ratios depend heavily on the exact nature of the fusing. Fibers fused under identical conditions sometimes yield quite different results. The general trend, however, is that the longer the tapering section of the coupler, the better the distribution uniformity, but at the expense of throughput efficiency. Some typical results are shown in Table 6-1.

We eventually had to settle for a compromise: reasonably good distribution and moderate loss (≤2 dB). If we label the four input ports as port 1 through 4 and the output ports as port 5 through 8, the best overall device has the characteristics presented in Table 6-2.

Table 6-1. Typical Coupler Characteristics

Coupler	Output Distribution (%) Port 1	Port 2	Port 3	Port 4	Insertion Loss (dB)
1	56	16	16	12	0.24
2	37	20	21	22	2.64
3	33	24	22	21	3.08
4	44	19	18	19	1.77

Table 6-2. Best Overall Device Characteristics

	Output Port No.	(dB)	Power Distribution Percentage
- Input Port No. 1	5	(-6.20)	24%
Insertion Loss	6	(-6.38)	23%
2.0 dB	7	(-5.69)	27%
	8	(-5.85)	26%
- Input Port No. 2	5	(-6.99)	20%
Insertion Loss	6	(-6.78)	21%
0.75 dB	7	(-6.78)	21%
	8	(-4.20)	38%
- Input Port No. 3	5	(-5.38)	29%
Insertion Loss	6	(-5.69)	27%
0.62 dB	7	(-6.02)	25%
	8	(-7.21)	19%
- Input Port No. 4	5	(-6.58)	22%
Insertion Loss	6	(-3.98)	40%
0.4 dB	7	(-6.99)	20%
	8	(-7.45)	18%

It is obvious that a 4 x 4 fused, biconical, tapered star coupler is by no means symmetrical. Both the power distribution and insertion loss depend on the input port number.

The star coupler is subsequently connectorized and installed in a packaging box. The final device is shown in Figure 1-3.

The multiplexer was characterized by coupling the output of a semiconductor laser to the connectorized fiber cable and sequentially connecting each of the four input ports of the multiplexer. Each time the four outputs were measured, the results are shown below.

Table 6-3. Multiplexer Characteristics

Loss \ Input Ports		1	2	3	4
Output Ports	5	-13.7 dB	-14.0	-13.0	-13.6
	6	-13.4	-13.5	-13.0	-12.6
	7	-12.3	-12.9	-13.2	-12.8
	8	-12.5	-12.8	-13.3	-13.5

It should be pointed out that the star coupler was made out of step-index fibers of 62.5 μm core diameter, while the fiber cables are 50 μm core graded index fibers. Therefore, the area mismatch loss between these two fiber types could be as much as 2 to 3 dB. The connectors will contribute ~1.5 dB of loss. In addition, the fusion process also introduces excess loss ranging from 0.4 to 2 dB. Thus, using the data given previously together with the various loss mechanisms accountable we can obtain rough agreement between the measured and the predicted values. It is interesting to note that the low loss ports are still the same before and after packaging.

We have also linked up the multiplexer with the demultiplexers, as shown in Figure 1-3. The measured overall throughput losses are found to be the sum of the individual losses of the multiplexer and the demultiplexers. There is a slight variation in the measured number due to connector losses.

SECTION 7

DISCUSSIONS AND CONCLUSIONS

One of the most troublesome aspects facing optical communications is laser noise due to power reflections. Whenever light is fed back into the laser in an optical fiber link, the laser output power will fluctuate. In some cases these fluctuations can be large enough to severely affect the system performance. There are several different possible mechanisms responsible for laser intensity fluctuations in different frequency ranges. As expected, the amplitude of the fluctuations increases as the reflection coefficient increases.

To reduce reflection-induced noise in lasers requires the reduction of the power fed back into the laser. One convenient way is to use an optical isolator. Other methods are to use fiber connectors with index matching liquids or to use a spherical fiber lens for input coupling. If a multimode laser is used, the feedback noise tends to be reduced because the total spontaneous emission power is increased and theory predicts better stabilization of the light output. Furthermore, a multimode laser will give rise to less modal noise (compared with a single mode laser) in multimode fiber optic link. Unfortunately these two advantages contradict the requirements for a low-insertion loss and high-crosstalk isolation multiplexer-demultiplexer design using dispersive elements.

When coherent sources are used in multimode fiber systems with mode selective loss, modal noise must be considered. It appears as unwanted amplitude modulation of the received signal and is very sensitive to physical distortion of the fiber or to laser wavelength changes. The noise, which can be lowered or raised by bending the fiber, may in practice seriously degrade digital system and completely disable analog systems.

Modal noise is produced by the interference pattern between the various propagating modes of the fiber, each of which is subjected to slightly different delays through the fiber caused by mode dispersion. A misaligned fiber joint can produce mode selective loss and change the interference pattern, resulting in time-varying fluctuations. The loss will vary both with changes in wavelength and with bending of the fiber before the misaligned joint.

If we consider the source coherence time (i.e., the time by which light may be delayed and yet still correlate or interfere with the undelayed light), it is clear that there can be no interference between any two modes in a fiber when the difference in their delays (i.e., intermode dispersion) is greater than the source coherence time, even though they are from the same source. The factors leading to increased levels of modal noise are:

- High source coherence (i.e., narrow spectral width). LEDs give lower modal noise because of their low spatial coherence.
- Mode selective loss. This occurs in misaligned joints, in mode selective dividers or taps, and even in unjointed fibers as a result of microbending loss.
- Small number of propagating modes (i.e., low NA, small core size, and graded as opposed to step index).
- Low mode dispersion.

Modal noise can be significantly reduced by using a low-loss joint; this may be sufficient to prevent excess noise in digital systems. The best solution appears to be the use of the lowest coherence source possible without introducing significant material dispersion penalty because of the broader spectrum. Long wavelength sources appear to be advantageous because of the lower fiber dispersion. However, there will be fewer modes for the same core diameter. We should also try to use the highest number of modes. It is highly advantageous to increase the number of modes by increasing the core diameter as this will give reduced joint losses for a given misalignment.

Unfortunately, in our demultiplexer design the optics of the device produce a one-to-one image of the input fiber end face at the output facet. Any wavelength error (or multimoding) of the source will result in increased insertion loss or crosstalk level. Therefore, from a low loss operation point of view, a single frequency source is desirable and temperature stabilization of each channel wavelength is a must. So care must be taken in the system interconnection to minimize reflection feedback as well as modal noise.

Our measured results presented in Section 5 indicated large insertion loss and a high crosstalk level from the demultiplexers. The reasons for the poor performance are combinations of factors:

- Errors in waveguide length during fabrication;
- Errors in output fiber array alignment during packaging;
- An inability to obtain better quality flexible gratings;
- Errors in fiber spacings in an array; and
- Lack of high quality semiconductor laser sources at the desired wavelengths.

As a matter of fact, some of the lasers used had a total emission width of ~40 Å, which is far too excessive considering that the adjacent channel wavelength is only 100 Å away.

We believe that wavelength separations of 100 Å are probably too ambitious for our device. The high resolution design actually made the device too sensitive to mechanical alignment and source wavelength stability. There is also room for improvement in the packaging design.

Nevertheless, under this program we actually carried out the design, development, fabrication and packaging of one multiplexer

and four demultiplexers. This accomplishment is significant, because for the first time we have a working device that is removed from the optical bench and the laboratory. Numerous novel ideas were incorporated into the device throughout the program. Hughes will continue to improve on the fabrication and packaging technology to correct for the poor insertion loss and crosstalk performance.

SECTION 8

REFERENCES

1. W.J. Tomlinson, "Wavelength Multiplexing in Multimode Optical Fibers," Appl. Opt. 16, 2180 (1977).

2. K. Aoyama and J. Minowa, "Optical Demultiplexer for a Wavelength Division Multiplexing System," Appl. Opt. 18, 1253 (1979).

3. T. Tanaka, H. Serizawa, and Y. Tsujimoto, "Simple Structure High Isolation Multi/Demultiplexer," Electron. Lett., 16, 869 (1980).

4. K. Nosu, H. Ishio, and K. Hashimoto, "Multireflection Optical Multi/Demultiplexer Using Interference Filters," Electron. Lett., 15, 414 (1979).

5. R. Watanabe and K. Nosu, "Slab Waveguide Demultiplexer for Multimode Optical Transmission in the 1.0 - 1.4 μm Wavelength Region," Appl. Opt., 19, 3588 (1980).

6. G.L. Tangonan, O.G. Ramer, H.R. Friedrich, C.K. Asawa, D.L. Pershini, and L.E. Gorre, Technical Digest of the Fifth European Conference on Optical Communications, p. 21, Paper No. 5-1, Sept., 1979, Amsterdam.

7. M. Born and E. Wolf, Principles of Optics, 5th ed. (Pergamon, N.Y. 1975), p. 412.

8. G.W. Stroke, Encyclopedia of Physics, Vol. XXIX Optical Instruments, (Springer-Verlag Berlin, Heidelberg, 1967), pp. 474-480.

1. Report No.	2. Government Accession No.	3. Recipient's Catalog No.
NASA CR-172429		

4. Title and Subtitle	5. Report Date
DEFINITION, ANALYSIS AND DEVELOPMENT OF AN OPTICAL DATA DISTRIBUTION NETWORK FOR INTEGRATED AVIONICS AND CONTROL SYSTEMS	June 1984
	6. Performing Organization Code
7. Author(s)	8. Performing Organization Report No.
H.W. Yen and R.J. Morrison	
9. Performing Organization Name and Address	10. Work Unit No.
Hughes Research Laboratories 3011 Malibu Canyon Road Malibu, CA 90265	11. Contract or Grant No. NAS1-15829
12. Sponsoring Agency Name and Address	13. Type of Report and Period Covered
NATIONAL AERONAUTICS AND SPACE ADMINISTRATION Washington, DC 20546	Final Report 1 May 79 - 31 Mar 84
	14. Sponsoring Agency Code

15. Supplementary Notes

Langley Technical Monitor: A. O. Lupton

16. Abstract

Fiber optic transmission is emerging as an attractive concept in data distribution onboard civil aircraft. Development of an Optical Data Distribution Network for Integrated Avionics and Control Systems for commercial aircraft will provide a data distribution network that gives freedom from EMI-RFI and ground loop problems, eliminates crosstalk and short circuits, provides protection and immunity from lightning induced transients and give a large bandwidth data transmission capability. In addition there is a potential for significantly reducing the weight and increasing the reliability over conventional data distribution networks.

Wavelength Division Multiplexing (WDM) is a candidate method for data communication between the various avionic subsystems. With WDM all systems could conceptually communicate with each other without time sharing and requiring complicated coding schemes for each computer and subsystem to recognize a message. However, the state-of-the-art of optical technology limits the application of fiber optics in advanced integrated avionics and control systems. Therefore, it is necessary to address the architecture for a fiber optics data distribution system for integrated avionics and control systems as well as develop prototype components and systems.

This report details the design, development, fabrication, and characterization of multiplexers and demultiplexers for multimode fiber optic applications.

17. Key Words (Suggested by Author(s))	18. Distribution Statement
Wavelength Division Multiplexing, Fiber Optics Planar Rowland Spectrometer, Grating Demultiplexer	Unclassified - Unlimited Subject Category 74

19. Security Classif. (of this report)	20. Security Classif. (of this page)	21. No. of Pages	22. Price
UNCLASSIFIED	UNCLASSIFIED	84	A05

N-305

For sale by the National Technical Information Service, Springfield, Virginia 22161

LANGLEY RESEARCH CENTER
3 1176 00518 2283